1985

THE SAN KAMPAENG GEOTHERMAL DEVELOPMENT PROJECT IN THE KINGDOM OF THAILAND

INTERIM REPORT

MARCH. 1986

JAPAN INTERNATIONAL COOPERATION AGENCY

1985

THE SAN KAMPAENG GEOTHERMAL DEVELOPMENT PROJECT IN THE KINGDOM OF THAILAND

INTERIM REPORT

MARCH. 1986

JAPAN INTERNATIONAL COOPERATION AGENCY

CONTENTS

Introduction

In FY 1984, as the third stage exploration of Geothermal Development Project in the San Kampaeng area of Northern Thailand, an exploration well, which was planned to have 1,500m in depth, was drilled by the JICA Study Team. Drilling work was smoothly carried on up to depth of 700m, however, because of a decrease of drilling speed, which was caused by hard rocks existed at deeper than 700m, drilling work was stopped at 1,227.3m in depth at the end of February, 1985.

From the results of geophysical logging which was carried out after drilling, it became clear that, compared with vertical distribution of resistivity obtained from MT method, higher resistivity was recorded, there were no permeable formations and that, contrary to expectation, low down hole temperature was measured.

Since such unexpected results of the drilled GTE-7, analysis of geophysical logging was reviewed and it was decided that fracture detection by geochemical survey called Fingerprint method would be carried out in and around geothermal manifestation area as the supplementary survey of the third stage exploration, in parallel with underground temperature survey at the depth of 100m conducted by the cooperation of EGAT.

Thus, this report is composed of two parts; the first paragraph describes analytical results of geophysical logging of GTE-7, and the second paragraph explains the results of fracture detection by geochemical survey and underground temperature survey, referring to the evaluation of geothermal reservoir in the San Kampaeng area and recommendation of drilling site of GTE-8 which will be drilled by EGAT in the near future.

I. Analytical results of logging in GTE-7

I. Analytical results of logging in GTE-7

1. Core survey

1-1 Geological structure revised by core survey

Fig. 1 and Fig. 2 show the geological map and geological section along E-W direction through GTE-2, respectively, which were compiled by geological survey in FY 1982.

The previous survey suggested that there might be an anticlinal axis of N-S direction running through near GTE-2. However, from the result of core survey of GTE-7, it was confirmed that this area is not characterized by anticlinal, but by monoclinal structure inclining to east side.

The revised geological map and geological section along E-W direction through GTE-7 are shown in Fig. 3 and Fig. 4, respectively. Moreover, one fault trending from NE to SW and running between GTE-2 and GTE-7 has been estimated. This is due to the reason that there may be a boundary which separates high temperature area from low temperature because down hole temperature of GTE-7 is too low to consider that of high temperature area. To confirm this matter, it is necessary to detect existence of the fault by other specific method such as geochemical survey.

2. Resistivity logging

2-1. Resistivity distribution in GTE-7

Distribution of resistivity and SP in GTE-7, which was cased upto 1,001m deep, is shown in Fig. 5. In Fig. 5, high resistivity is recorded at depth of 540 - 570m, 700 - 770m, 805 - 830m, 865 - 890m and 910 - 950m in both long and short normals, while others are lower than 100Ω-m. At the deeper portion than 1,001m, high resistivity is seen at depth of 1,010 - 1,030m, 1,175 - 1,215m and 1,220 - 1,227m at bottom of hole.

Resistivity distribution in GTE-7 is characterized by alternation of high and low resistivity zones. Among them, there are some high resistivity zones where long normal shows higher than 500Ω-m, especially at depth of about 1,200m, it shows higher than 2,500Ω-m.

Judging from high resistivity distribution and decrease of drilling

speed, it can be understood that the Palaeozoic formations in this area are composed of extremely hard rocks.

2-2 Correlation of MT survey with resistivity logging in GTE-7.

By the single shot survey to measure the azumith and inclination of GTE-7 conducted upon completion of drilling, the trajectory of the well is estimated to have deviation of 160m - 173m at the bottom of hole.

The result of correlation of trajectory of the well with vertical profile of resistivity obtained from MT survey revealed that GTE-7 did not pass through a low resistivity zone of 3Ω-m indicated by MT survey and that the bottom of hole is in a zone having low resistivity level of 26 - 36Ω-m.

Left side of Fig. 6 shows correlation of trajectory of the well with MT survey result.

On the other hand, right side of Fig. 6 illustrates the correlation of resistivity logging with MT survey. Analytical results obtained from the correlation are summerized as follows:

(1) Result of logging shows wide dispersion of resistivity ranging from several ohm-m up to several thousands ohm-m. Judging from the resistivity distribution obtained from MT survey, it is understood that only low resistivity portion which is included in the alternation composed of low and high resistivity layers is reflected. In general, MT survey has such tendency that in the area consisting of high and low resistivity layers, result of measurement is not indicated by the mean value, but by relatively low resistivity values.

(2) Comparing resistivity distribution obtained from resistivity logging with that from MT survey, it seems that rough correspondence is observed, although the former has higher values than the latter.

(3) The effect of rock alteration distributed around the geothermal manifestation area is considered as another reason that MT survey shows relatively low resistivity values.

3. Temperature logging

3-1. Hole temperature in the exploration wells drilled by EGAT and GTE-7.

Hole temperature of each exploration well is shown in Fig. 7 and that of GTE-7 is shown in Fig.8. Characteristics of each hole temperature are as follows:

GTE-1 ------ Conductive type, temperature gradient at deeper than 470m : 10°C/100m (1°C/10m).

GTE-2 ------ Convective type, thermal water of 1ℓ/min is discharging, maximum temperature is 107°C at 300m deep.

GTE-4 ------ Conductive type, temperature gradient at shallower than 280m : 8°C/100m (1°C/12.5m), at deeper than 280m : 18°C/100m (1°C/5.5m). That difference may be due to conductivity of rocks.

GTE-5 ------ Conductive type, temperature gradient : 12°C/100m (1°C/8.3m).

GTE-6 ------ Convective type, steam and hot water are flowing out, well-head temperature : 103°C, bottom hole temperature: 118°C at 490m.

GTE-7 ------ Linear distribution of hole temperature, temperature gradient : 4°C/100m (1°C/25m), lost circulation occurs at 1,005m deep, temperature anomaly is due to recharge of thermal water contained in Alluvial deposits near the surface.

3-2. Analysis of temperature logging in GTE-7

(1) Recharge and discharge areas in geothermal system

In the area where geothermal system is formed, there exists discharge area with high heat flow and recharge area with low heat flow.

In the former, underground temperature is high because of effect of ascending hot water, but temperature gradient is low in the portion where convection is formed, while in the latter, underground temperature is low because of descending cold water and also temperature gradient is low.

(2) Conceptual hydrothermal system in the San Kampaeng area

Geothermal system in the San Kampaeng system is included in the area located between Huai Pong Fault trending from NNW to SSE and Huai Khu Ha Fault with the same direction as Huai Pong Fault.

The area with active geothermal manifestations is regarded as the discharge area of ascending hot water as shown in Fig. 9.

Judging from the conceptual geothermal system in the San Kampaeng area and characteristic down-hole-temperature curve in GTE-7, it may be considered that GTE-7 drilled the recharge area of thermal water located around geothermal manifestation area.

3-3 Calculation of formation temperature affected by descending thermal water

When water percolates to some depth from the ground surface through a pipe (fissure) with small diameter, a bottom hole temperature of the pipe is calculated by the following formula:

$$\theta_b = \theta_o'' + \alpha D - \frac{\alpha}{\gamma} [1 - \exp(-\gamma D)]$$

θ_b : water temperature at the bottom of pipe
θ_0'' : initial temperature of percolating water
α : temperature gradient
D : depth

$$\gamma = \frac{2\pi\gamma_0 h''}{a\rho c}$$

a : amount of percolating water
ρ, c : specific weight and heat of water
γ_0 : radius of pipe (fissure)
h'' : cooling coefficient

In the recharge area, it is considered that original heat flow of rocks and geologic formations gets decreased because of percolating of cold water. Based on the idea that hole temperature of GTE-7 presents that of geologic formations cooled by percolating water, some kind of matching has been tried. That is, under what kind of condition does the percolating water temperature show the actual recorded temperature of GTE-7.

Each value used for matching is as follows:

α : 1°C/9m (same as that of GTE-5)

γ_0 : small pipe with radius of 2 cm (fissure)

θ_0'' : 60°C (underground temperature of GTE-7 at 150m deep, regarded as temperature of percolating thermal water)

a : 20 ℓ/min (amount of lost circulation at 1,005m deep)

ρ, c : 1 g/cm^3, 1 cal/cm^3 · °C

h'' : 0.25×10^{-3} cal/cm^3· sec.·°C

The result of calculation is shown in Fig. 10.

From the result of calculation, distribution of temperature by matching is similar to that of hole temperature of GTE-7. As a conclusion, it can be said that temperature distribution of GTE-7 presents that of the recharge area where thermal water with 60°C is percolating.

4. Conceptual model of geothermal system modified by the result of drilled GTE-7

Before drilling of GTE-7, it had been considered that GTE-7 would be drilled in the discharge area of hot water, which was indicated by the low resistivity zone less than 5Ω-m(Fig. 11). However, in accordance with the result of drilling of GTE-7, the characteristic down hole temperature curve indicates that the drilling site is in the recharge area of thermal water.

Consequently, the model of geothermal system had to be changed as follows; the discharge area, that is, the extent of the geothermal reservoir with hot water is limited to the southern area of the estimated fault trending from NE to SW.

The conceptual model of geothermal system modified by the result of drilling of GTE-7 is shown in Fig. 12.

5. Summary and future work plan

By the geological survey conducted in FY 1982, it was considered that there is an anticlinal axis near GTE-2 trending from north to south. However, the result of core survey conducted in 1985 suggested that geological structure in the area with drilling site of GTE-7 is not anticlinal, but monoclinal, inclining to east side. Also, because of the reason that the area with drilling site of GTE-7 is regarded as the recharge area characterized by low down-hole-temperature and low temperature gradient, it was estimated that there may be a fault with north-east direction between GTE-7 and geothermal manifastations area.

Based on the result of resistivity logging in the GTE-7 hole, the correlation of resistivity distribution in the GTE-7 with that obtained from two-dimentional analysis of MT method was undertaken. As the result of correlation, it was known that alternation of high and low resistivity zones is correlated to low resistivity zone of MT method. This is due to the reason that, in the case of MT method, the effect of low resistivity zone in alternation consisting of high and low resistivity zones is strongly reflected, then MT method can not detect high resistivity zone if there exists high resistivity zone in alternation.

As known from the correlation of resistivity logging with two-dimentional analysis of MT method, the bottom hole of GTE-7 is considered to be situated outside of low resistivity zone estimated by MT method because of a small inclination of drilled hole.

Contrary to expectation, it was found that the down-hole-temperature was only 100°C at the bottom hole of 1,227m, although the drilling site of GTE-7 is located near geothermal manifestation area.

From the analysis of characteristic temperature curve in the drilled hole showing that the down-hole-temperature at the bottom is only 100°C, while near-surface-temperature at depth of 150m is 60°C, that is, showing remarkable low temperature gradient, it was concluded that the area with drilling site of GTE-7 is regarded as the recharge area of thermal water with water temperature of 60°C which comes from the geothermal manifestation area.

Although extent of the recharge area is not clear, it is estimated that a fault located between drilling site and geothermal manifestations with north-east direction may play a role as the boundary between recharge and discharge areas.

As a conclusion, it can be said that useful data to evaluate geothermal reservoir could not be obtained from drilling of GTE-7, although the conceptual model of geothermal system in this area was constructed. Therefore, in order to understand geothermal reservoir, it is necessary to do supplementary survey in FY 1985.

For this purpose, it is recommended that fracture detection and underground temperature survey at depth of 100m are carried out in and around the discharge area, that is, in the manifestation area as future work plan. If EGAT is intended to do drilling of GTE-8 exploration well in this area in future, a recommendation of drilling site of GTE-8 will be made based on the results of the supplementary survey.

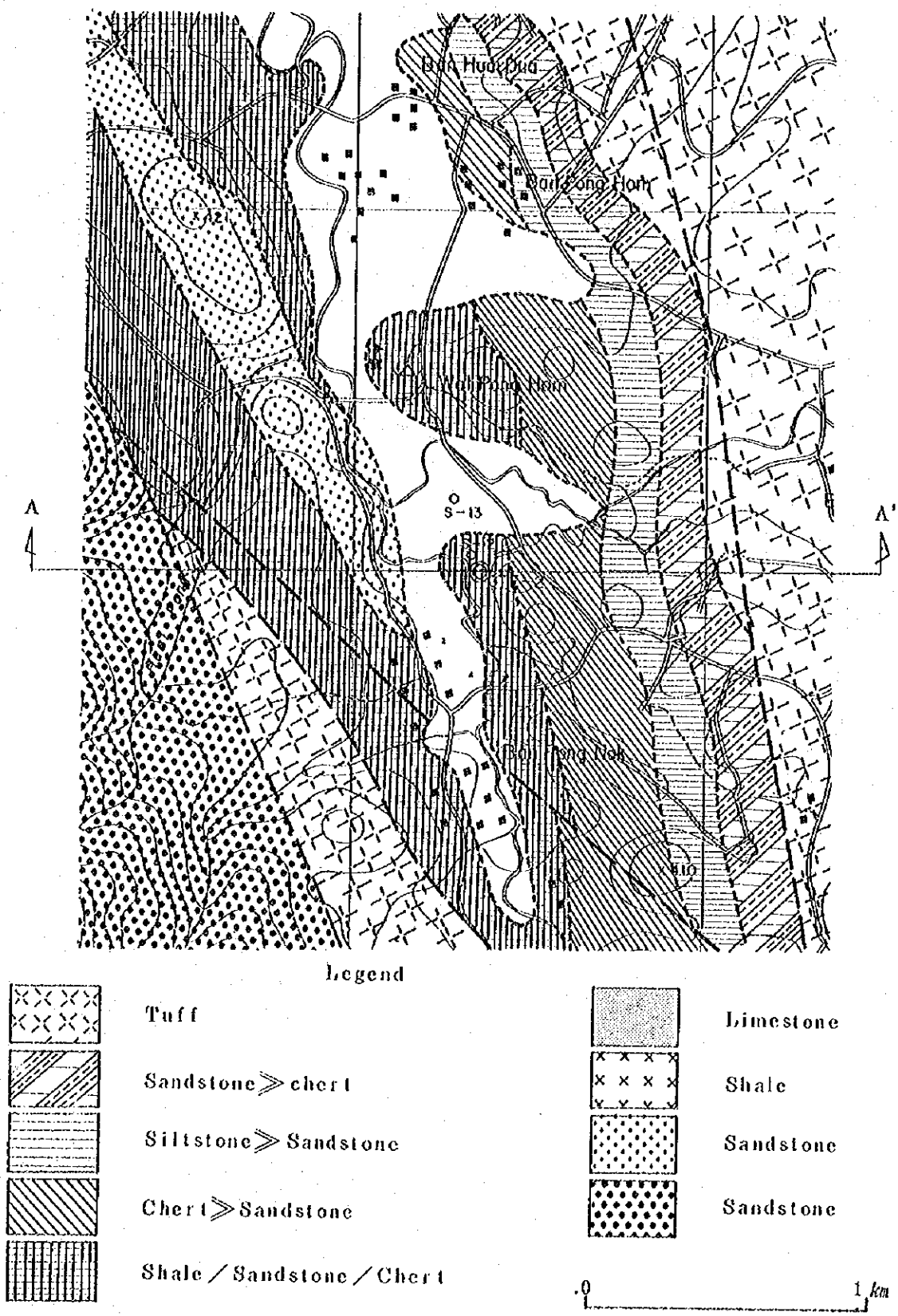

Fig. 1 Geological map made in FY 1982

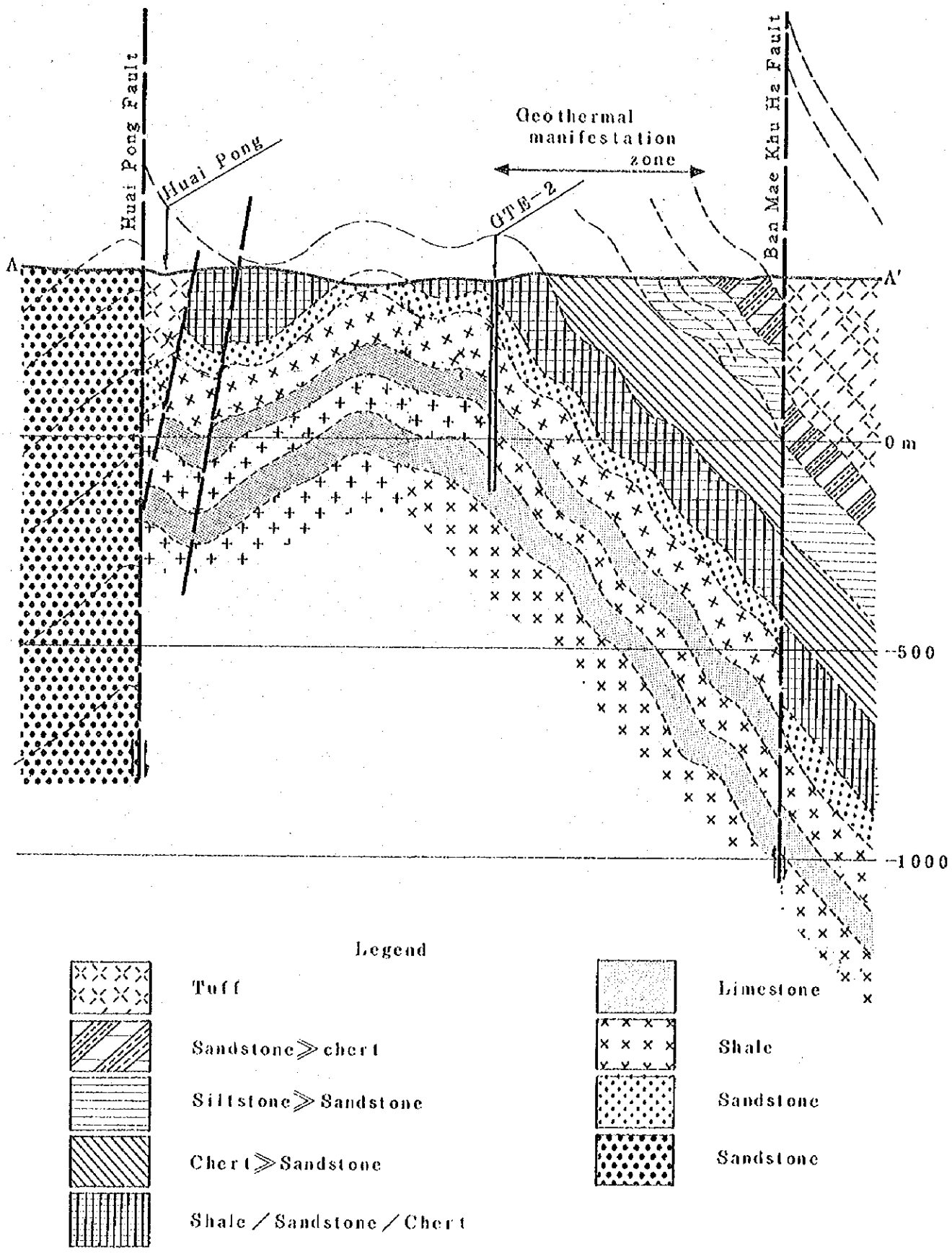

Fig. 2 Geologic section along E - W direction through GTE-2.

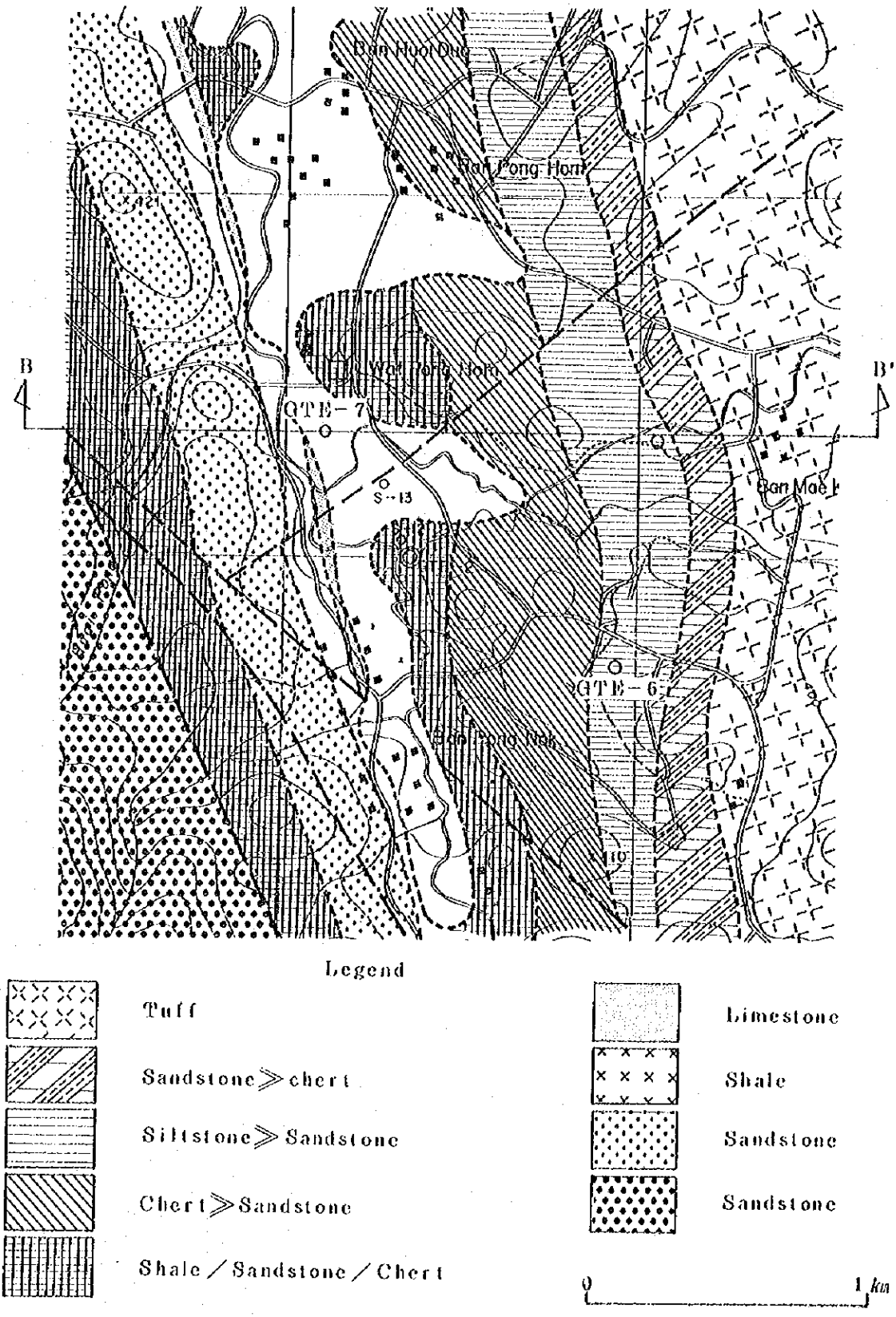

Fig. 3 Geological map revised by the result of core survey of GTE-7.

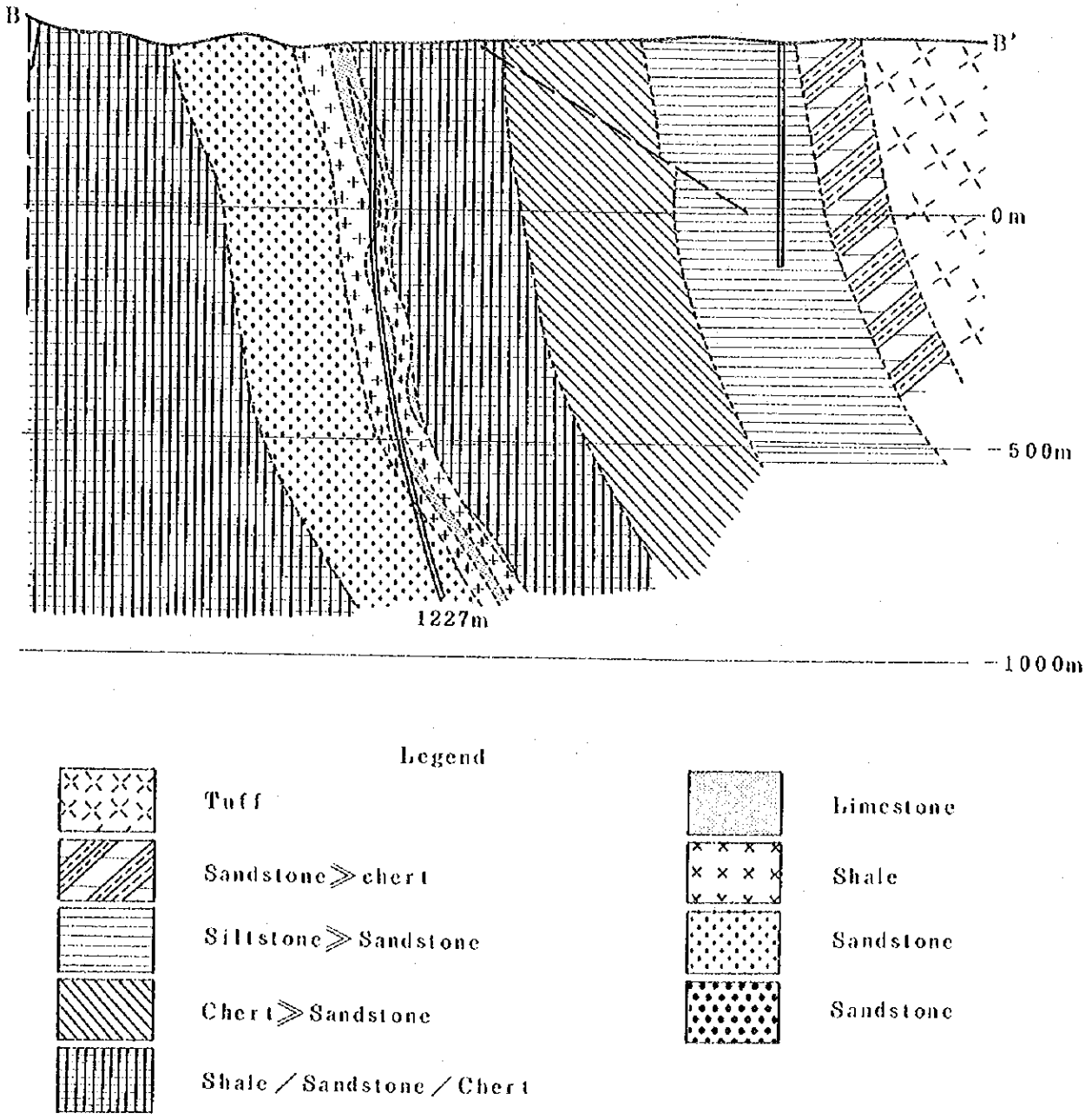

Fig. 4 Geologic section along E - W direction through GTE-7.

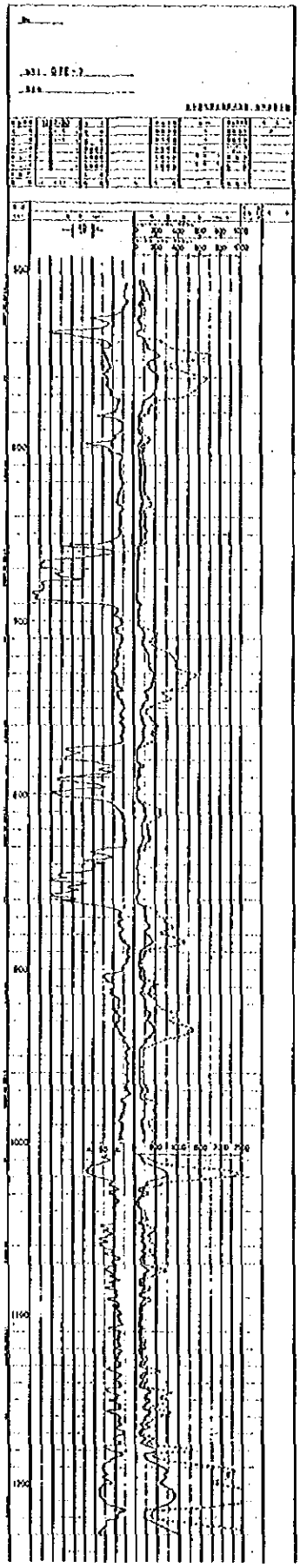

Fig. 5 Record of resistivity logging in GTE-7.

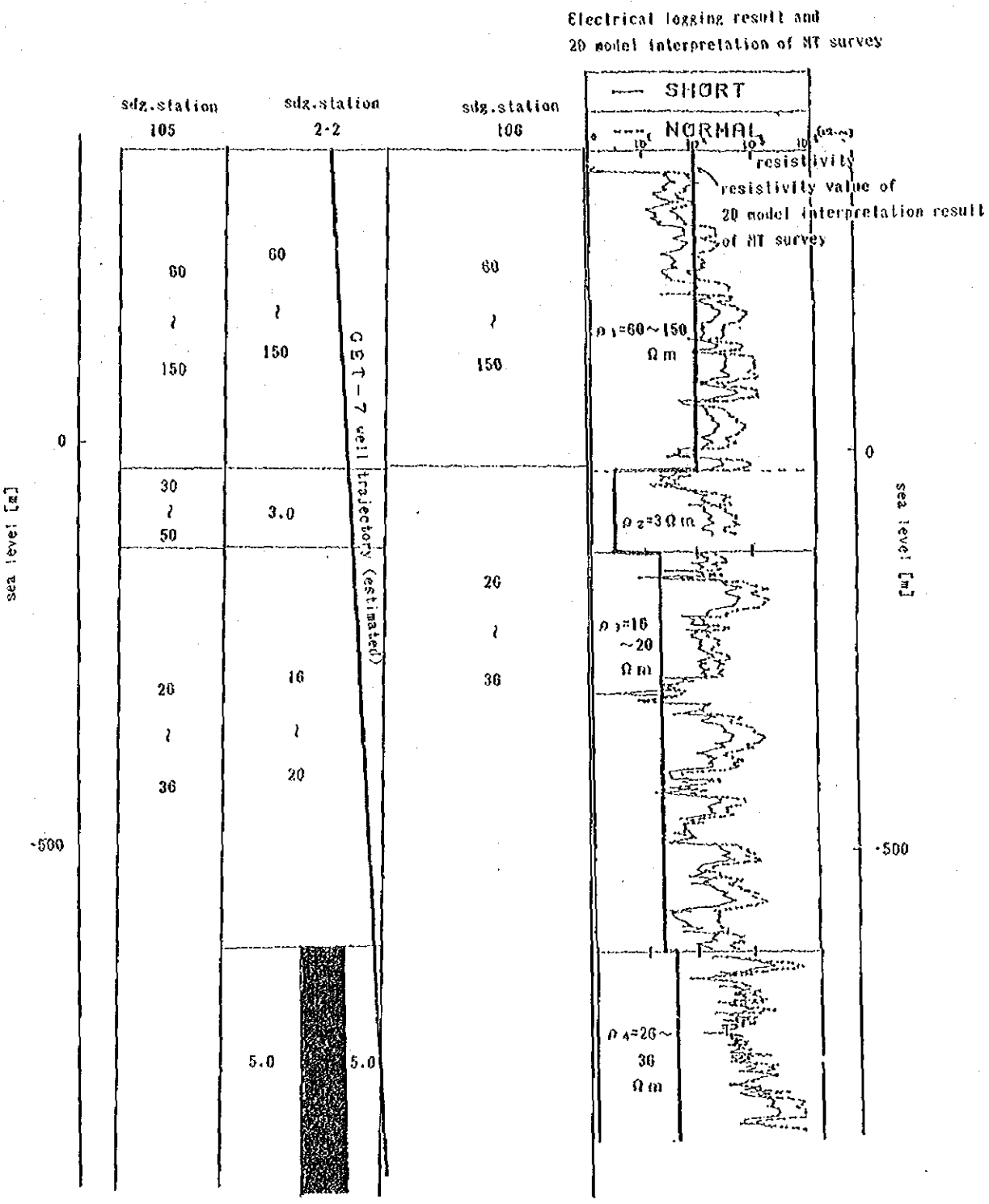

Fig. 6 Correlation of resistivity section by MT method with resistivity logging in GTE-7.

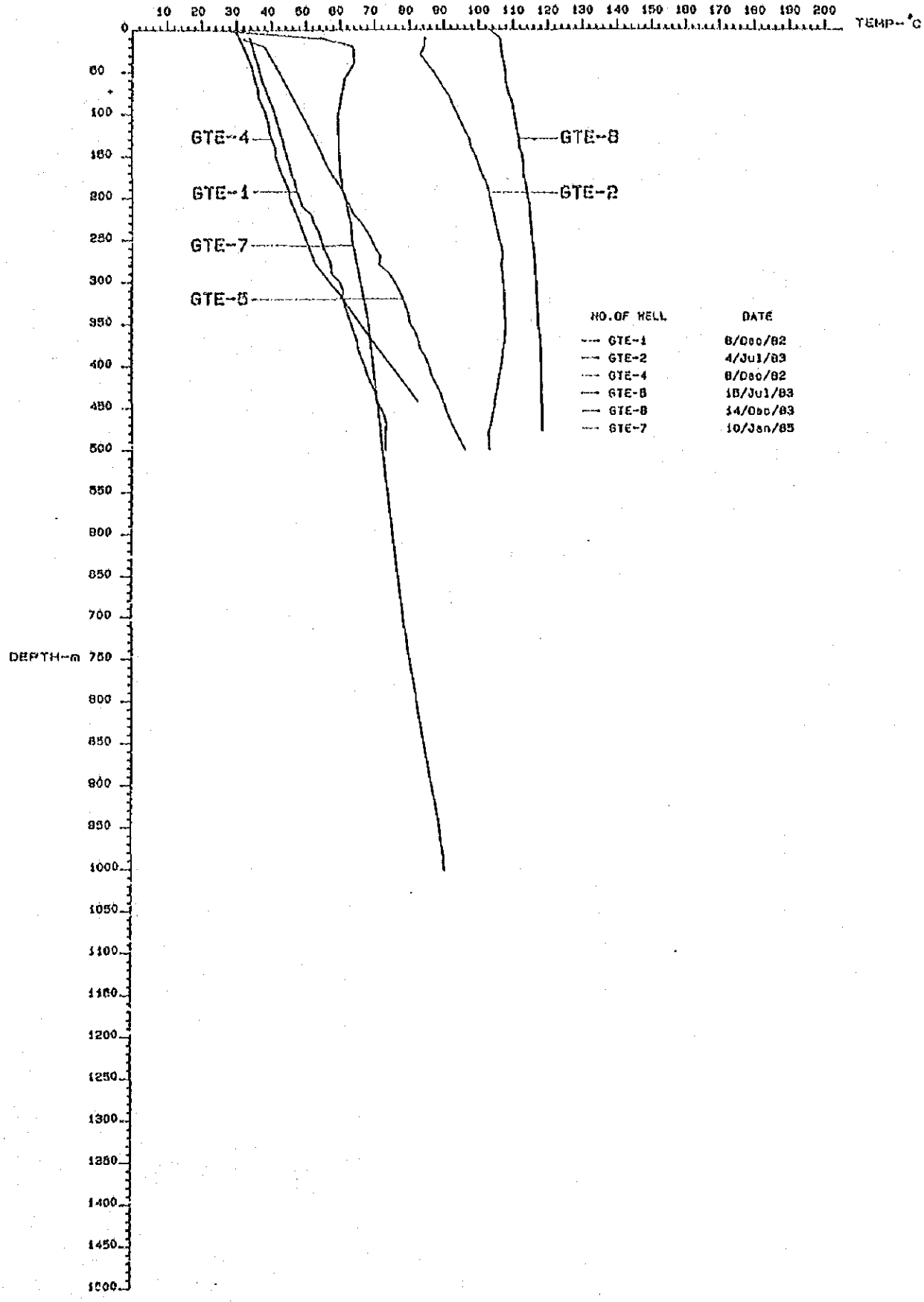

Fig. 7 Vertical temperature distribution in the exploration wells drilled by EGAT and GTE-7.

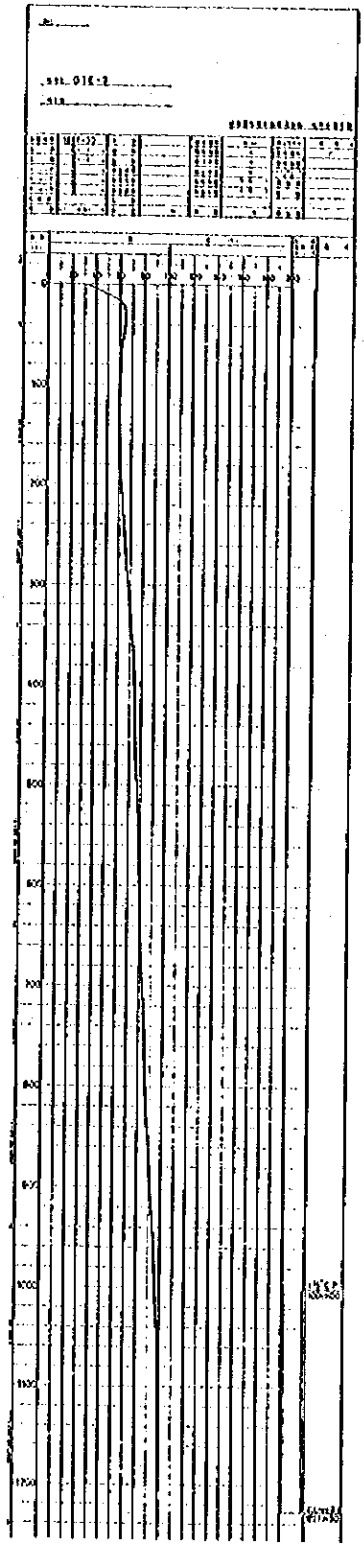

Fig. 8 Record of temperature logging in GTE-7.

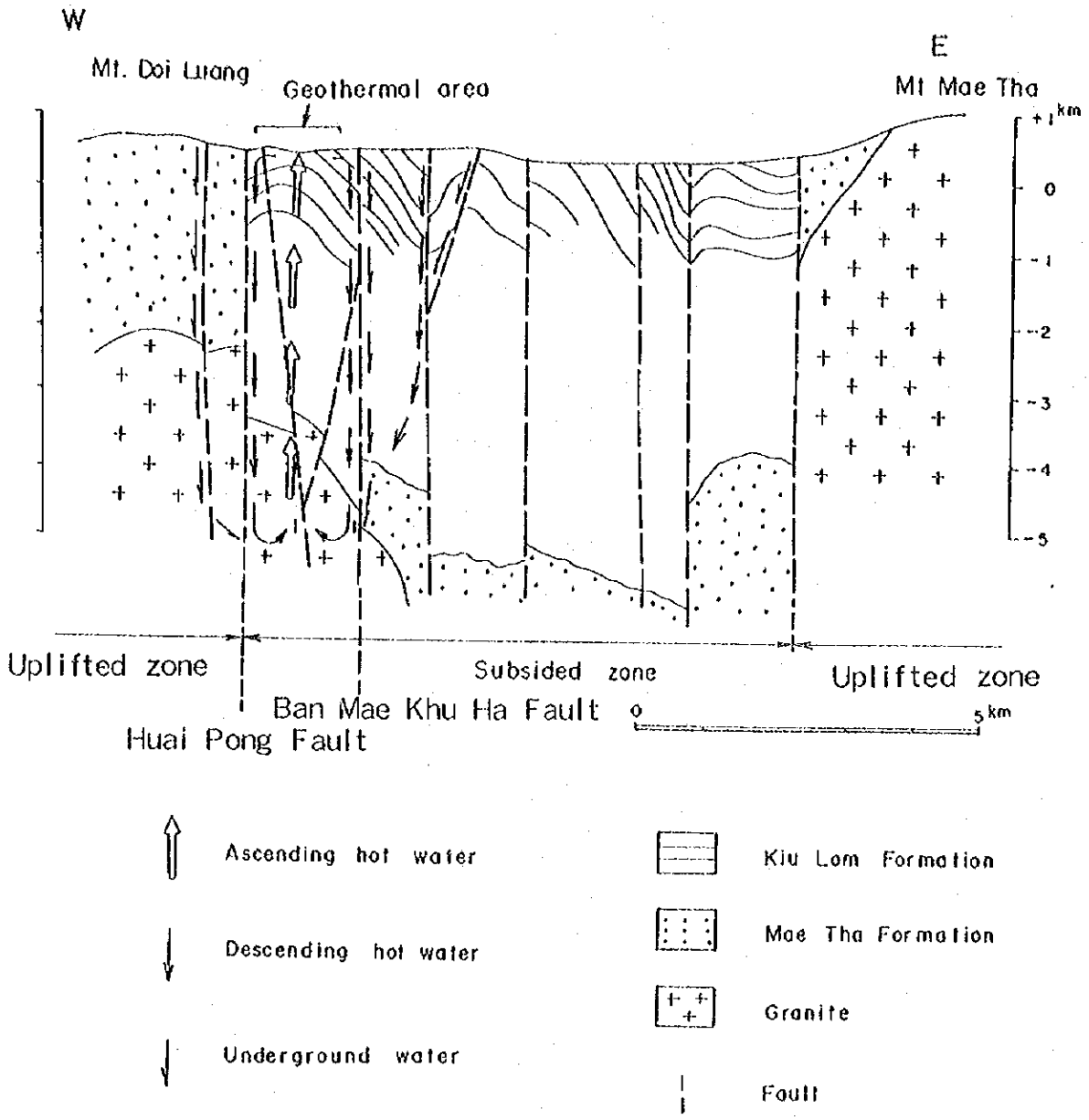

Fig. 9 Geothermal system in the San Kampaeng area.

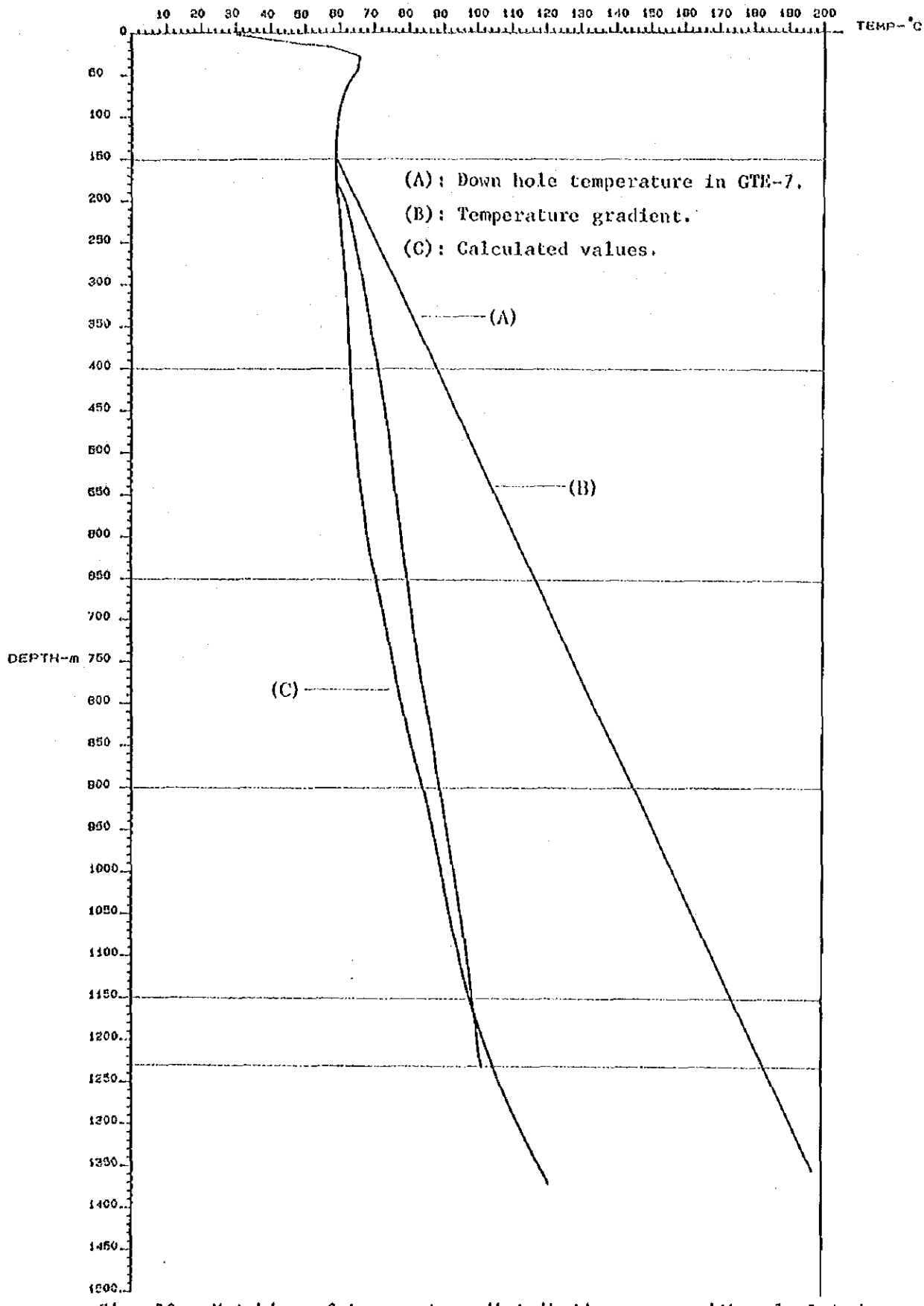

Fig. 10 Matching of temperature distribution curve with calculated temperature distribution curve in the recharge area.

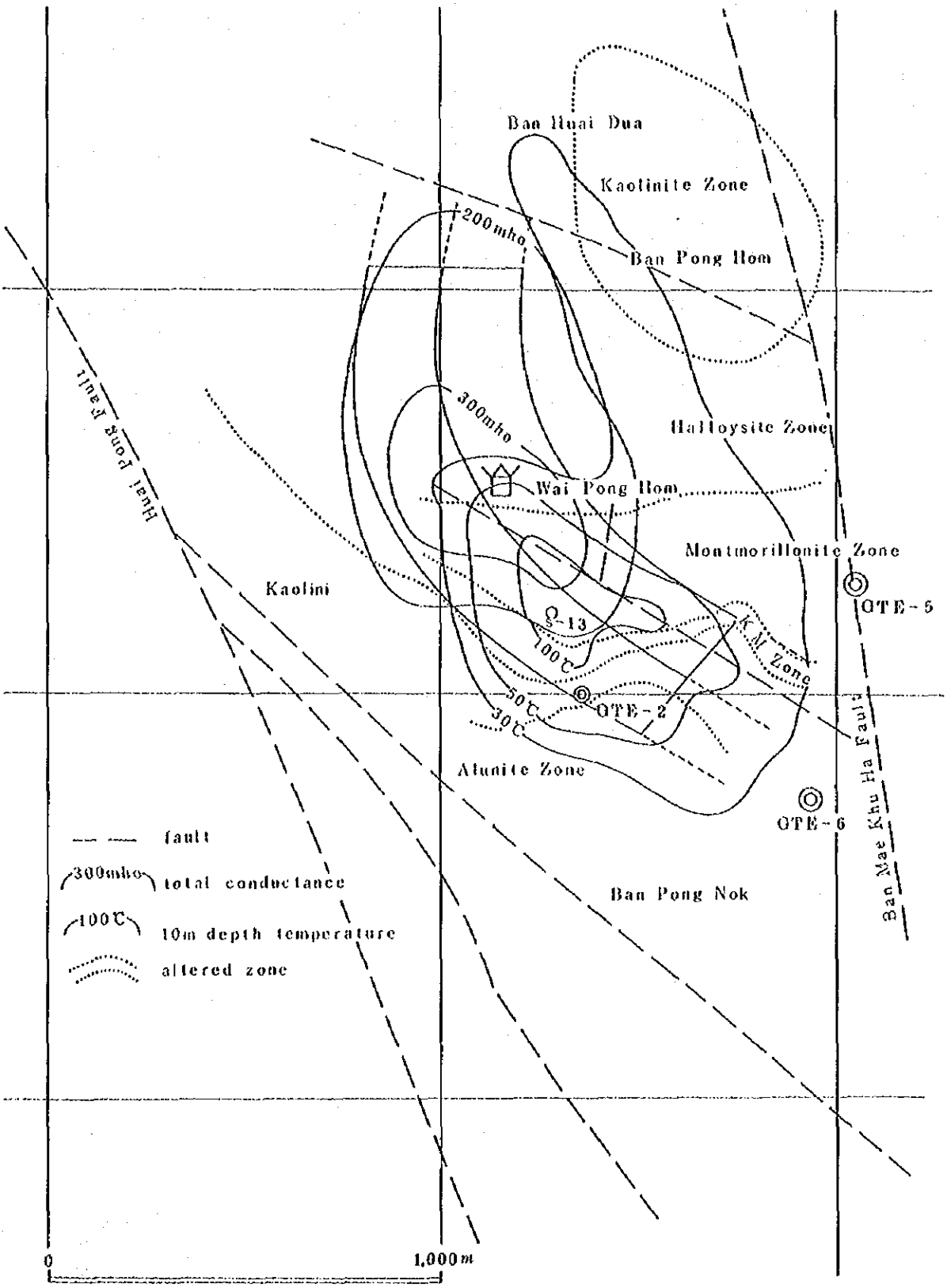

Fig. 11 Conceptual model of geothermal reservoir estimated before drilling of GTE-7.

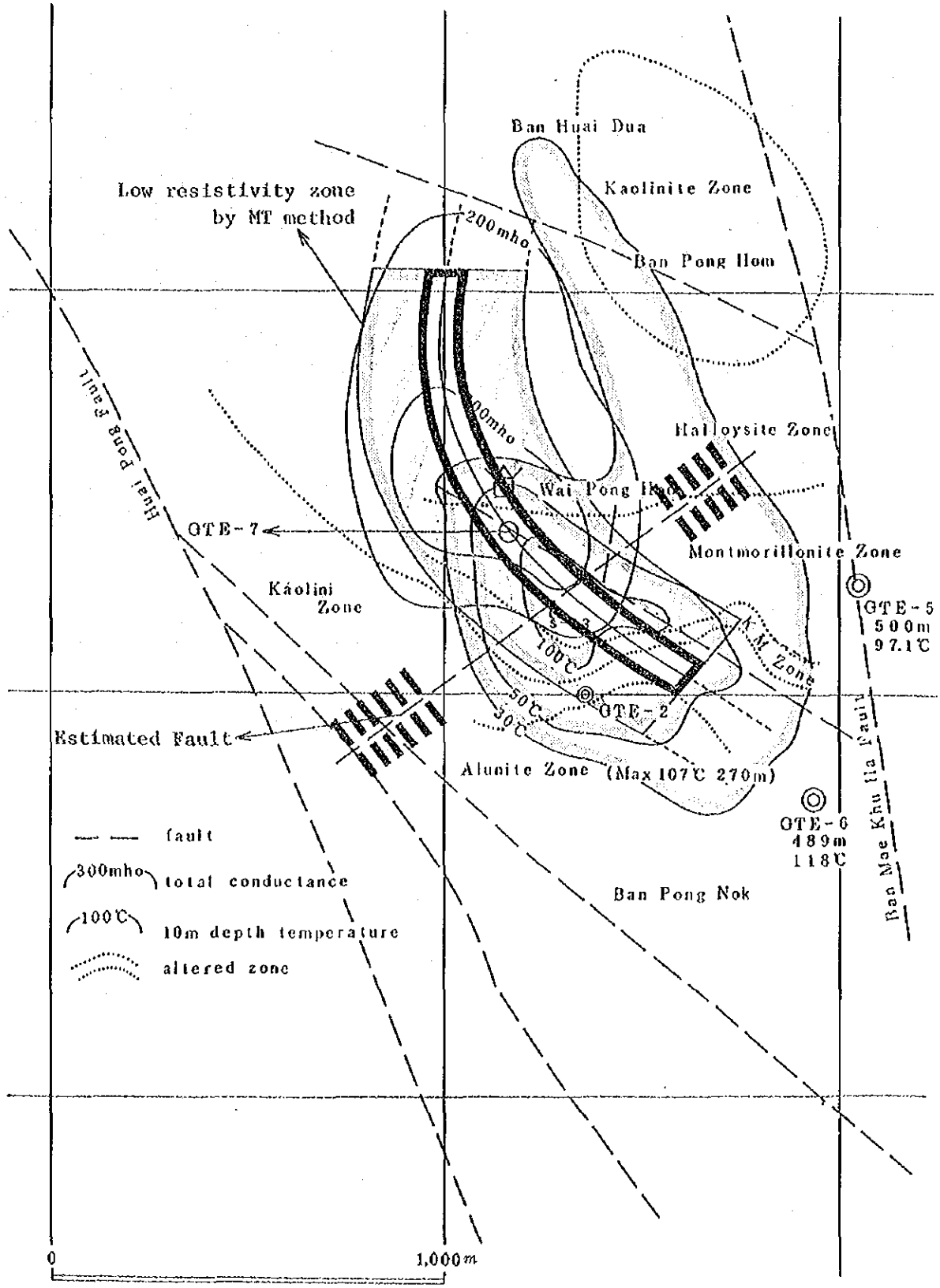

Fig. 12 Conceptual model of geothermal system modified by the result of drilling of GTE-7.

Ⅱ. Results of supplementary survey of the third stage exploration

II. Results of supplementary survey of the third stage exploration

1. Objectives of the survey

As the third stage exploration, drilling of an exploration well, GTE-7, of 1,227.3m deep was carried out by JICA in FY 1984.

However, since the result of drilling was not successful to obtain useful data to evaluate geothermal reservoir in the San Kampaeng area, analysis of geophysical logging in GTE-7 was undertaken after completion of drilling.

Based on the analytical results of logging, it was scheduled that as supplementary survey of the third stage exploration, a fault or fracture detection and an underground temperature survey in the discharge area with geothermal manifestations would be carried out in FY 1985.

Objectives of the survey are to confirm the extent of the geothermal reservoir in the San Kampaeng area, to examine if another exploration well which is planned to be drilled by EGAT in the near future is worth drilling and to locate GTE-8 for EGAT if good results would be obtained.

The fault or fracture detection was carried out by JICA study team by using geochemical survey called Fingerprint method.

In paralell with the fault or fracture detection, the underground temperature survey at depth of 100m was undertaken by the cooperation of EGAT.

For this purpose EGAT drilled 10 heat holes and measured down-hole-temperature to make iso-thermal contour line map at depth of 100m.

2. Fault or fracture detection by Fingerprint geochemistry

2-1. Introduction

Application of gas geochemistry to fault and fracture detection is based on the principles that fault and fracture can be an open path for gases emanating from deep underground. Detection of such seepage is the objective of gas geochemistry method. Gases such as CO_2, Hg, He, Rn are analyzed as indicator gases in conventional geochemical method.

The practical application of gas geochemistry is complicated by a number of problems. Meteorological factors influence gas emission rates. Seasonal and daily variations of gas emmision rate at a single location can be as large as a factor of 50. Surface condition of ground also influences gas emission. Further there is no single gas component effective for detection of fault and fracture in any cases.

The geochemical technique chosen for this study is the fingerprint technique developed at the Colorado School of Mines which can compensate most of the disadvantages of the conventional method. The technique is an integrative soil-gas technique utilizing pyrolysis-mass spectrometry (Py-MS) with multivariate statistics. Its main features can be summarized in the following two points.

(1) Integrative gas collection by activated charcoal to avoid temporal variation of gas emission.

(2) Interpretation of gas pattern by multivariate statistics rather than concentration of single gas component.

It is considered that this new method can provide valuable information regarding fault and fracture in the survey area.

2-2. Method of study

2-2-1. Field sampling

Gas collector used for sampling consists of a small ferromagnetic wire with activated carbon affixed to the end contained in a glass culture tube sealed by a teflon lined cap. Activated carbon serves as a collector and integrator for soil gas. Figure 13 shows gas collector used in the survey.

Gas collectors are transported to the field in sealed condition and a hole approximately 30cm deep is dug with small hand auger. The cap is removed from the tube and the tube is placed, open end down, into the hole. Soil is filled and packed around the tube and the hole is filled to ground level. The sample sites are marked by pushing a small piece of plastic flagging tape into the fill soil.

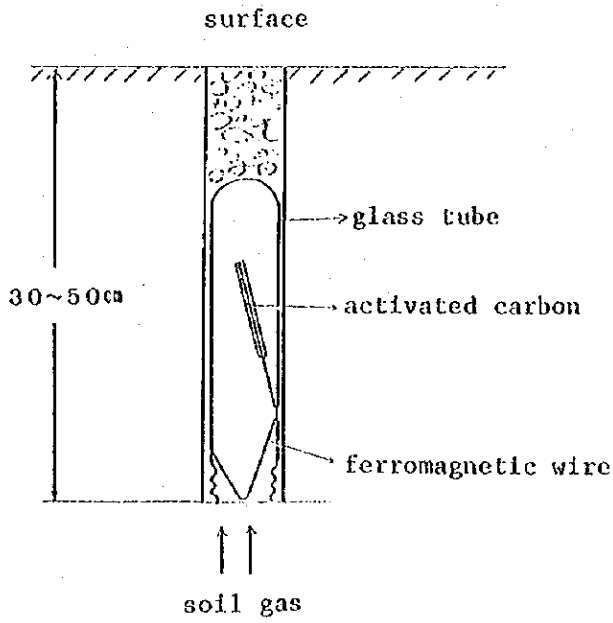

Fig. 13 Gas collector

Approximately 10 days after emplacement, the collectors are retrieved in the same order as emplacement to ensure that residence time is as uniform as possible. The retrieved collectors are sent to the laboratory for analysis.

2-2-2. Laboratory Analysis

Analysis of collected soil gases on ferromagnetic wire is performed by computerized pyrolysis - mass spectrometer for gases of mass range from 29 to 240. Figure 14 illustrates a schema of the mass spectrometer system.

Ferromagnetic wire is headed by high frequency electromagnetic source (Curie point pyrolyzer) to desorb soil gases from activated carbon. The composition of wire controls the temperature the heater attains, thus clean reproducible heating for desorption of the trapped compound is performed.

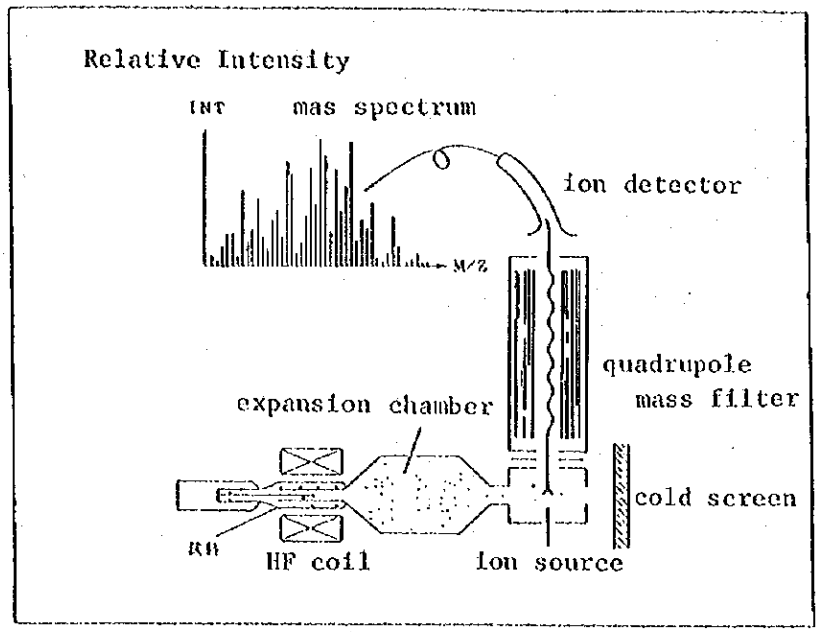

Pyrolysis-Mass Spectrometry System

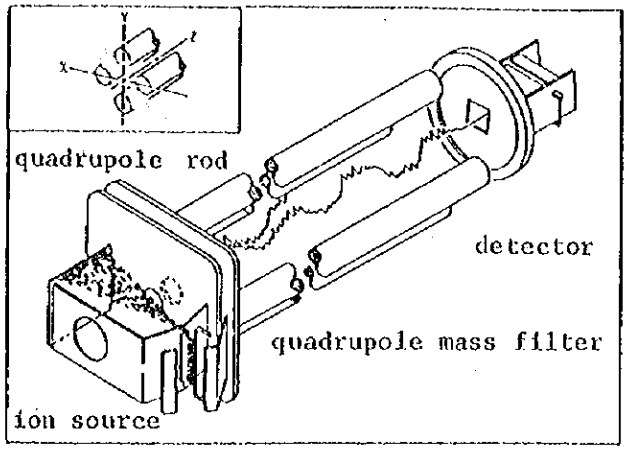

Quadrupole Mass Filter

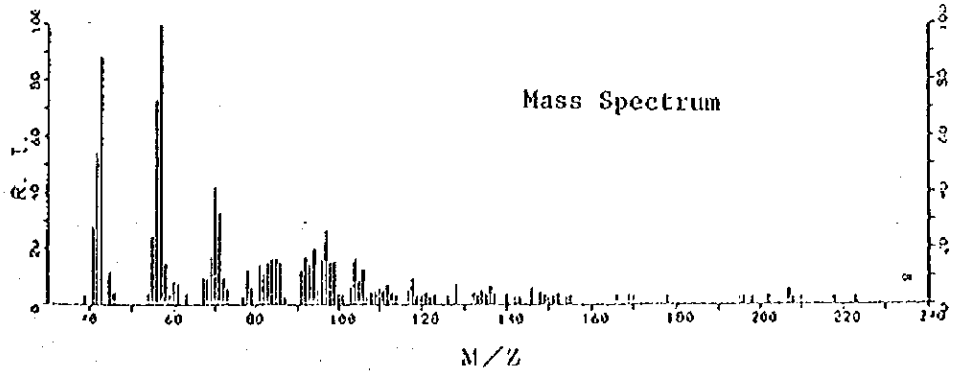

Fig. 14 Pyrolysis mass spectrometry and mass spectrum

The desorbed gases from the pyrolyzer are analyzed by quadrupole mass spectrometer. Gas molecule are ionized by electron impact and then enter into the quadrupole mass filter. Depending on certain parameters, ions of particular m/z (mass of the ion/charge of the ion (normally unity)) values undergo stable oscillations and emerge from the mass filter to be detected by an electron multiplier. Mass scanning up to 240 are achieved.

The obtained mass spectral data can provide information regarding absolute flux as well as relative abundance of different gases. Example of mass spectrum is shown in figure 14. Horizontal axis represents m/z value and vertical axis shows its relative intensity which is normalized by the strongest intensity of the spectrum as 100%. Since the mass spectrum is a characteristic signature of the soil gas, it is called "fingerprint".

2-2-3. Data interpretation

(1) Fault/fracture fingerprint

(i) Fault/fracture characteristics

The presence of high molecular weight components in a fingerprint (generally $m/z \geq 120$) has correlated to faults and fractures. This suggests high molecular weight gases which are less movable can reach the ground surface if there is open passage by fault and fracture.

Following are typical fingerprints indicating the presence of fault and fracture (Fig. 15).
Some fingerprints are identified as fault and fracture indication even without the presence of high molecular weight gases. Fig. 16 is example of such fingerprint. Heavy component shows stronger peak intensity than lighter one whereas the background fingerprints exhibit opposite tendency. In this case, comparison with background fingerprint is important.

Fault and fracture trend can be mapped on the basis of these fault and fracture fingerprint distribution.

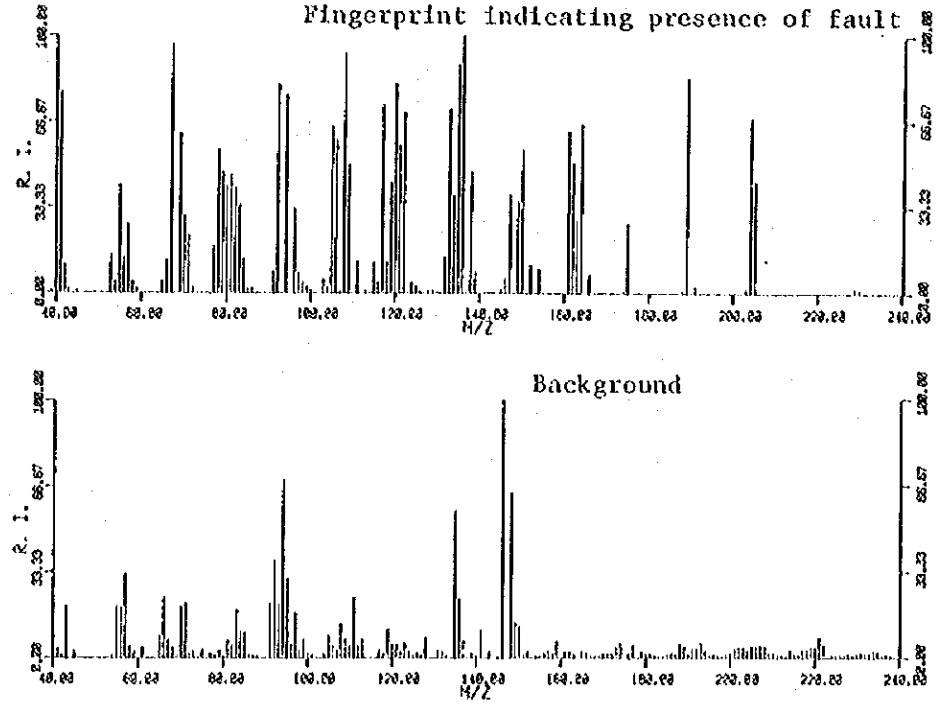

Fig. 15 Typical fault/fracture fingerprint (1)

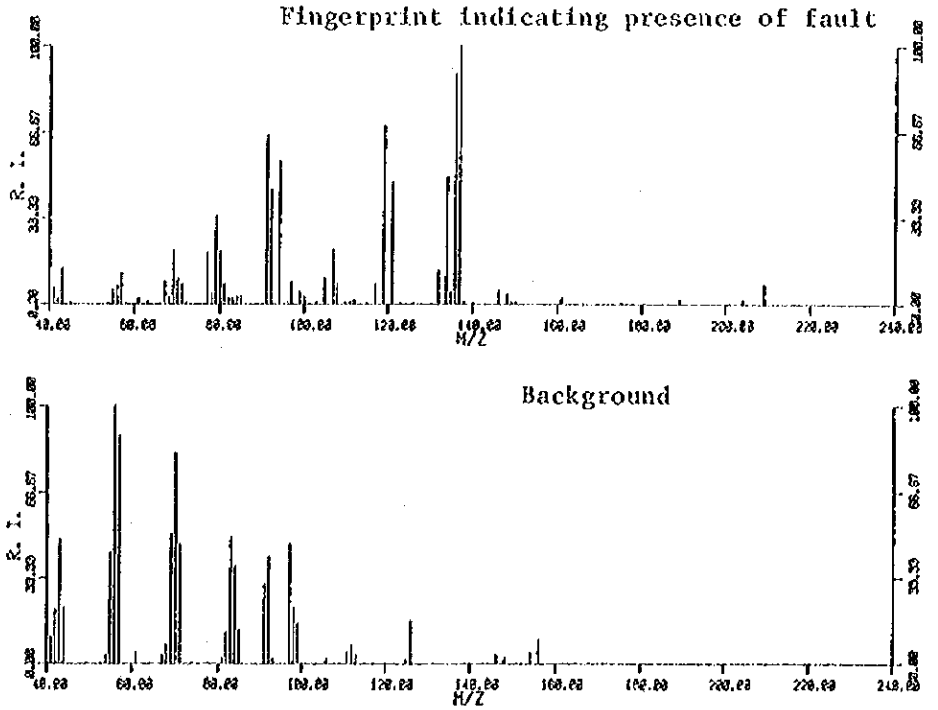

Fig. 16 Typical fault/fracture fingerprint (2)

(ii) High molecular weight gas ratio

In addition to qualitative inspection of mass spectrum by eyes, quantitative comparison of high molecular weight gas ratio is effective interpretive tool to locate fault and fracture. Here high molecular weight gas ratio is defined as follows.

$$\text{HIGH MOLECULAR WEIGHT GAS RATIO} = \frac{\Sigma \text{ ion intensity of } m/z \geq 120}{\text{Total modified ion count}} \times 100$$

Comparison of the ratio can provide subjective support to the visual identification of fault and fracture fingerprint as well as to their relation on plane surface.

(2) Gas flux analysis

The ion intensity appeared on mass spectrum is proportional to the number of molecules collected by the sampler, thus comparison of gas flux rate is achieved by comparing ion intensity.

For this purpose, TMIC (Total Modified Ion Count) is calculated by substracting the influence of atmospheric noise from total ion intensity of the mass spectrum. In other word, TMIC represents gas flux rate from underground at the point.

It is supposed that gas flux rate increases if underground gases are emanating through fault and fracture.

(3) Similarity analysis by multivariate statistics

Another method of data interpretation is pattern classification of fingerprint by computer aided multivariate statistics. This method is based on the hypothesis that gas composition would not be affected considerably by factors such as rock type, soil, vegetation and other surface condition since none of these factors appears to have a preferential effect on certain component, whereas absolute gas flux rate would be affected by them. If different gas source (i.e. petroleum or geothermal) were present in underground, the surface gas composition (= pattern of fingerprint) related to them can be readily discriminated. Thus pattern classification by fingerprint similarity would be able to locate geothermal reservoir, and fault/fracture which has close relation to geothermal reservoir.

For carrying out multivariate statistical analysis, mass spectrum data of each sample are transformed to data vector in multidimensional space as follows,

$$X_i = (X_{i1}, X_{i2}, \ldots\ldots\ldots\ldots, X_{in})$$

here X_{i1} is the ion intensity of the i-th sample at the first m/z value and X_{i2} is the ion intensity at the second m/z value and so on.

Then Euclidean distance between each data vector would be calculated as follows.

$$D_{ij} = \left[\sum_{k=1}^{h} (X_{ik} - X_{jk})^2 \right]^{1/2}$$

The distance is a measure of dissimilarity between samples. For example, four samples in three components system can be analyzed as follows. The calculated distances between samples and three dimensional plots of data vectors are shown in figure 17.

	Component A	B	C
Sample No.1	30.0	60.0	10.0
No.2	29.0	61.0	10.0
No.3	14.0	50.0	36.0
No.4	70.0	20.0	10.0

Obviously sample No.1 and No.2 are very similar among four samples and calculated distance clearly indicates this relation.

In practical application, similarity or distance from the model samples, which are thought to represent characteristic fingerprint of the target, is calculated and compared. If good model samples are not available, background samples will be used as anti-model to find area of abnormal fingerprint.

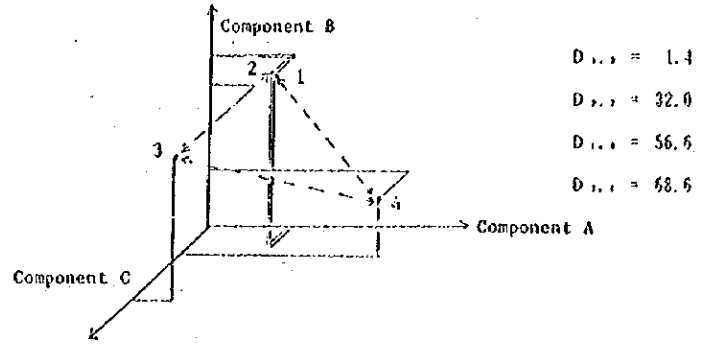

Fig. 17 Distance of four samples in three dimentional space.

2-3. Results

2-3-1. Field procedure

Sampling sites were determined prior to the emplacement of the gas collectors by survey using compass. Total number of sampling sites are 359. Sampling sites are arranged as combination of lines (20m spacing) and grids (100m spacing).

The gas collectors were emplaced at all 359 points. 24 collectors were either lost or damaged, thus number of recovered gas collectors for analysis remained 335.

Fig. 18 shows the sampling points.

2-3-2. Data interpretation

(1) Fault/fracture fingerprint

(i) Location of fault/fracture fingerprint

Mass spectrum of all samples were inspected for fault and fracture characteristics as mentioned at data interpretation. As a result, following 41 samples were identified as fault/fracture fingerprint.

No. 4, 8, 11, 13, 28, 36, 56, 59, 68, 93, 96,
103, 125, 129, 134, 140, 166, 186, 190, 211, 221, 228,
229, 245, 248, 251, 254, 257, 263, 269, 302, 304, 306,
307, 322, 324, 335, 347, 351, 354, 258

Several typical fingerprints of above mentioned samples are shown in comparison with their background fingerprint. (Fig. 19).

Distribution of above mentioned 41 samples are shown in Fig.20. Considering continuity and linearity of the distribution and their relation to topography, following arrangements were assumed to be probable fault and fracture.

NW-SE system

166 - 245 - 257 - 306,307 - 335
134 - 228 - 248 - 269 - 351
56 - 125 - 190
13 - 96 - 221 - 263

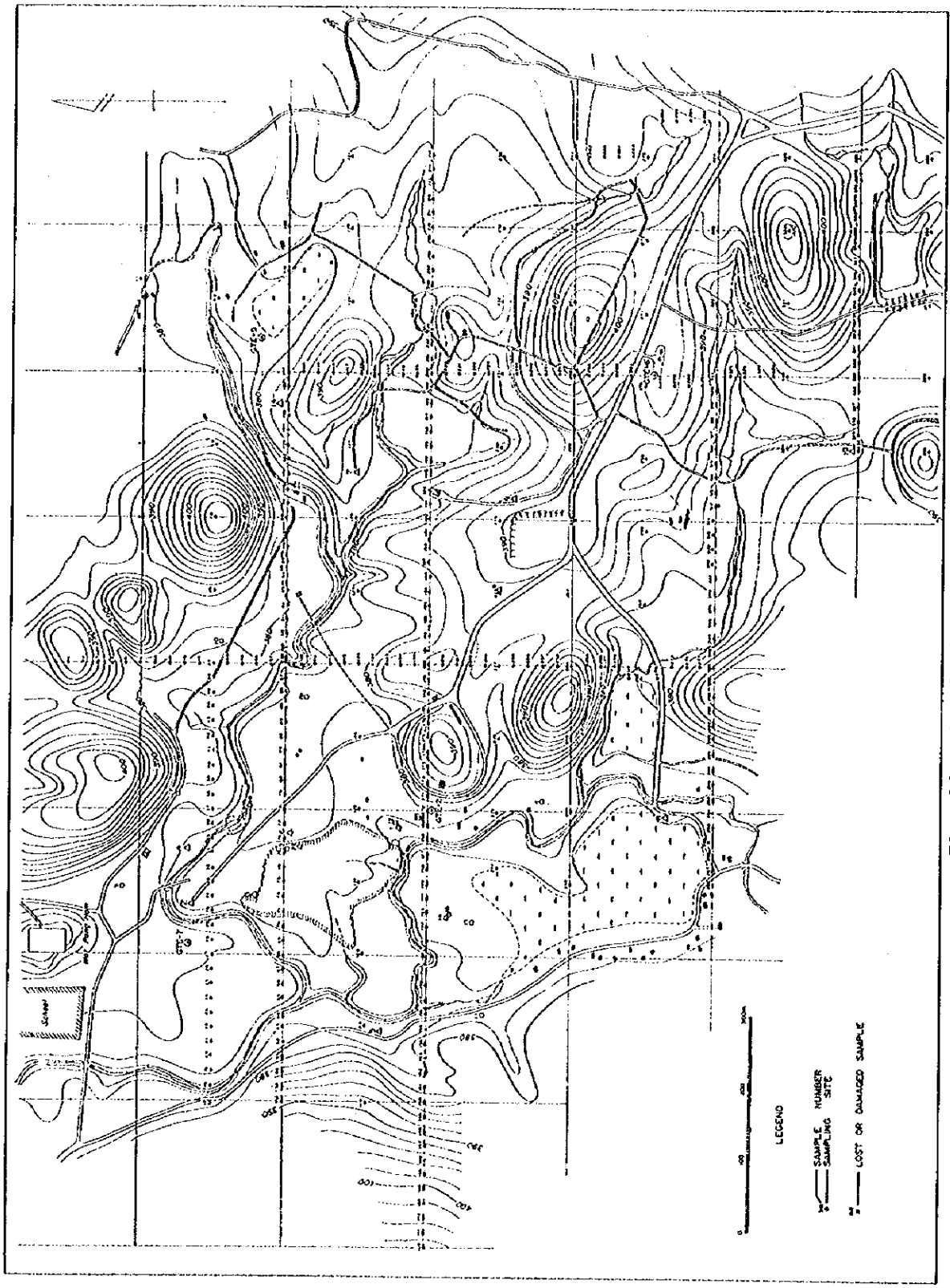

Fig. 18 Sample location map.

NE-SW system

4 - 28 - 59

4 - 36 - 68 - 140

11 - 103 - 125 - 134

N-S system

93 - 125 - 186 - 228

190 - 229 - 248

(4) High molecular weight gas ratio

Contour map of high molecular weight gas ratio is shown in Fig. 21. Fig. 21 also includes location of fault and fracture fingerprint.

High molecular weight gas ratio ranges from 0% to 44%. However, nearly half of the samples shows ratio of 0% and thus average of the ratio remains 2.3%. Area of the ratio higher than 2.5% is shown as anomaly in Fig. 21.

Fig.21 indicates two features of the area. First, the western half of the area shows lower ratio than the eastern half. This is probably due to the difference of lithology rather than fault or fracture distribution. Second, two anomalous zones run parallel to NW-SE trend from the southeastern edge of the area. Narrower zone of the above mentioned anomalous zones at the southern side coincides well with the previously assumed NW-SE arrangement (166 - 245 - 257 - 306,307 - 325). Wider zone at northern side seems to represent the NW-SE arrangement (134 - 228 - 248 - 269 - 351) and the N-S arrangement (92 - 125 - 186 - 228 and 190 - 229 - 248). Low ratio zone run parallel to the wider anomalous zone on its north side. It is interesting to note that boundary of the high and the low ratio zone coincides with the assumed NW-SE arrangement (13 - 96 - 221 - 263). There is no NE-SW trend observed in Fig. 21.

(2) Area of high total gas flux

The lowest gas flux at the area is 4,656 (ion count) and the highest is 1,083,756 (ion count). The average gas flux is 81,259 (ion count). Contour map of total gas flux is shown in Fig. 22. Area of flux higher than

100,000 ion count is shown as high total gas flux zone.

Fig. 22 suggests following. Similar to the distribution of high molecular weight gas ratio, the western half of the area shows relatively low gas flux. This may be explained by difference of lithology.

High flux zone of NW-SE trend elongates from the southeastern edge of the area. This zone coincides very well with the high molecular weight gas anomalous zone and includes the NW-SE arrangement and the N-S assumed arrangement. Accordingly, this zone may reflect presence of fractured zone. There are several scattered high flux areas at the northern side of this zone. They seem not to have any obvious trend. At the southern side of this zone, there is another high flux zone of NW-SE trend. This zone deviated to south from the NW-SE assumed arrangement (166 - 245 - 257 - 306,307 - 335).

High flux zone presents also at the northwestern side of the area. This area locates at the intersection of the NW-SE assumed arrangement (166 - 245 - 257 - 306,307 - 335) and the NE-SW assumed arrangement (4 - 36 - 68 - 140). In addition, there is high flux zone showing NE-SW trend at the western edge. These high flux zones suggests presence of an NE-SW fault at the northwestern side of the area.

(3) Similarity analysis by multivariate statistics

Model samples were chosen from the surface manifestation area where temperature at 20m depth is above 70°C. Originally the model samples were supposed to represent characteristic gas pattern related to geothermal of the area. However, as a result of computation, it was found that the model samples did not possess common unique fingerprint among them but scattered abnormal fingerprints each other. Therefore they were not suitable for further consideration for similarity analysis.

Then samples representing background fingerprint were chosen as anti-model in order to locate area of abnormal gas emanation related to geothermal activity. Fig. 23 shows distance (= dissimilarity) contour map by the computation based on anti-model. Larger distance indicates more abnormal gas pattern. The samples showing fault and fracture fingerprint possess extremely large distance value. If they were included in contouring process, general trend of the area would be ignored by their local high anomalous zones. Therefore they were eliminated from contouring process to get general trend of the

area. Area of distance larger than 5 are shown as anomaly in Fig. 23.

The largest anomaly in Fig. 23 includes the surface manifestation area at the north of GTE-2, and extends to the southeast side of the area. This indicates that the source of abnormal gas pattern may be in the southeast of the surface manifestation area.

It is noted that the anomalous zone at the surface manifestation area seems to be restricted its extension by the previously assumed NW-SE arrangement (166-245-257-396,307-325) and NE-SW arrangements (4-36-68-140 and 11-103-125-134). This suggests that these assumed arrangements are faults which limit spread of geothermal fluid.

The southeast extension of the anomaly seems to be along with the N-S arrangement (93-125-186-228) and the NW-SE arrangement (134-228-248-269-351). This suggests that these assumed arrangements are faults which act as path of geothermal fluid.

2-4. Discussion

2-4-1. Geological structure of the area

This area is underlain mainly Permian Lower Kiu Lom Formation, which consist of alternating layers of sandstone, shale, chert, limestone and basaltic tuff. The formation is lithologically divided into sandstone bed, alternating bed of limestone and shale, sandstone bed, shale predominant bed, sandstone predominant bed, alternating bed of sandstone and shale, shale predominant bed and basaltic tuff bed in ascending order. Relationships between each beds are inferred to be conformity (Fig.24).

Since these beds trend north-northwest and steeply (more than 50°) dip to east, monoclinic structure eastward has been assumed as a whole. However, short pitched anticlines and synclines having north-south axis are recognized in this formation.

The lowest sandstone bed and alternation bed of limestone and shale are recognized only in deeper part (depth more than 200m) of GTE-2 and GTE-7 drilling holes. Therefore, the existence of major anticline is expected at the western margin in this area.

Though no faults are recognizable at the surface in this area due to the bad exposure, faults of NW-SE system and of NE-SW system are assumable by the distribution of formations and other geological factors. As for the NW-SE system, fault passing from the northern central part to the southeastern part through between GTE-5 and GTE-6, and fault running from the northwestern part to the south central part through westside of GTE-2 have been assumed. As for NE-SW system, fault running from the central west margine to the central north margine through between GTE-7 and GTE-2 has been presumed.

2-4-2. Geological consideration of the result

The geological survey and drillings suggest existence of the monoclinic structure and faults of NE-SW system and NW-SE system. Geological interpretation on the results of this supplementary survey is summarized as follows.

(1) Location of fault/fracture fingerprint

Sixteen out of fourty-one location of fault/fracture fingerprint lie on the geologically assumed fault. This supports the presence of three faults. These faults are considered as comparatively large fault. Seventeen of the remains of fault/fracture fingerprint lie in the area surrounded by these faults. Inside this area, there are NW-SE, NE-SW, N-S tendency of distribution of fault/fracture fingerprint indicating small faults or fractures.

(2) Total gas flux

Distribution of high flux zone suggests presence of fault and fractured zone. Especially high flux zone in the area surrounded by the three major faults implies close relation of fault system and ascent of geothermal fluid.

(3) Similarity analysis

Scattered abnormal gas pattern are detected in the area surrounded by the three major faults including the surface manifestation area. This suggests geothermal source presents at the southeast of the area and geothermal fluid ascends through fractured zone in the area.

/

2-5. Summary

Geochemical survey by fingerprint technique was conducted to locate fault and fracture in the area. Three hundreds and fifty-nine gas collectors were emplaced and 335 of them were recovered for analysis.

Data interpretation of the survey suggests following.

(1) Fourty-one out of 335 samples shows fingerprint characteristics of fault and fracture. Considering the distribution of 41 samples, following fault and fracture are assumed.

NW-SE system : 166 - 245 - 257 - 306,307 - 335
134 - 228 - 248 - 269 - 351
56 - 125 - 190
13 - 96 - 221 - 263

NE-SW system : 3 - 28 - 59
4 - 36 - 68 - 140
11 - 103 - 125 - 134

N-S system : 93 - 125 - 186 - 228
190 - 229 - 248

Especially two NW-SE arrangements (166 - 245 - 257 - 306,307 - 335 and 134 - 228 - 248 - 269 - 351) and NE-SW arrangement (4 - 36 - 68 - 140) are considered to be comparatively large faults.

(2) Anomalous zone of the contour map of high molecular weight gas ratio support the presence of the above mentioned NW-SE faults.

(3) The contour map of total gas flux shows high flux zone lies in the area between the above mentioned NW-SE arrangements and the NE-SW arrangement. This suggests presence of the above mentioned NW-SE faults and the NE-SW fault.

(4) Zone of abnormal gas pattern detected at the surface manifestation area elongates to southeast suggesting ascent of geothermal fluid from the southeast of the manifestation area.

Locations of faults assumed by the geochemical survey agree well with that of the geologically assumed faults. The survey results suggest ascent of geothermal fluid through fractured zone at the southeast of the manifestation area.

3. Underground temperature survey

3-1. Drilling of heat holes

The survey was carried out by cooperation of EGAT.

In paralell with fault or fracture detection by Fingerprint method, for the purpose of underground temperature survey at depth 100m, drilling of heat holes was commenced from July, 1985.

The purpose of underground temperature survey is to make iso-thermal contour line map and to know the relation between fault or fracture distribution and underground temperature distribution. For this purpose, drilling of heat holes were arranged to be distributed in the survey area of fault or fracture detection. Locality map of heat holes is shown in Fig. 25. Among 10 heat holes, one is located 850m south of the survey area, therefore that hole is not included in Fig. 25.

Due to the reason that if hot or thermal water is discharged from the hole, down hole temperature does not indicate formation temperature, but that of discharged fluid, fractures with lost circulation were filled by cement, and moreover, iron casing pipe was inserted to bottom of hole so that temperature disturbance does not occur in the hole. Two examples of completion of drilled holes are shown in Fig. 26.

3-2. Measurement of down hole temperature

After drilling of each heat hole was finished, down hole temperature was measured in several times. Fig. 27 shows vertical temperature distribution in each hole which was made by using data obtained after long standing time more than one month. Table 1 shows bottom of hole temperature in each heat hole.

In addition to heat holes, drilled exploration wells GTE-2, -5, -6 and -7 are located in and around the survey area. Among them, GTE-2 and -6 have discharge of hot water, then, not showing formation temperature because of dynamic state. On the other hand, others are under static state with long standing time. Then, data on down hole temperature of these exploration wells are regarded as formation temperature at depth of 100m. The data also shown in Table 1 were used to make isothermal contour line map.

3-3. Relation between underground temperature distribution and fault or fracture distribution

Based on the data presented in Table 1 , iso-thermal contour line map higher than 60°C was drawn as shown in Fig. 28. Fig. 29 shows a map putting fault or fracture distribution over underground temperature distribution. The facts known from the distribution map shown in Fig. 29 are as follows,

(1) The high temperature zone with above 60°C is nearly coinsides with the area occupied by two faults with NW-SE direction and direction of the high temperature zone is comformable with that of the faults.

Extention of the high temperature zone to north side is cut off by a fault with direction of NE-SW which means that the fault plays a role as boundary between high and low temperature zones. From the result of drilling of GTE-7, it was estimated that a fault might be existed between GTE-7 and geothermal manifestation area which separates high temperature zone (discharge area) from low temperature area (recharge area). From the result of the survey carried out in FY 1985, it can be said that the idea has been supported by the result of the survey.

(2) High anomalous areas in the temperature distribution map are found in two portions: one in the geothermal manifestation area and another at south of the manifestation area. This fact coinsides with the result of analysis of Fingerprint method. In particular, from the fact that No.9 heat hole shows high temperature of 112°C, it is possible to say that hot geothermal fluid may be reserved in the area with extent of wider than 500m and longer than 1,000m which lies between two faults with NW-SE direction.

(3) As conclusion, it is summerized that occurrence of the geothermal reservoir in the San Kampaeng area has become clear by the results of fault or fracture detection and underground temperature survey.

4. Conceptual model of the geothermal reservoir obtained from the results of the surveys

In the geothermal area such as San Kanpaeng composed of hard rocks, geothermal fluid in the underground moves through crack along faults or fractures. So, the target area of geothermal development is limited to the area with dominant fractures.

Geochemical survey such as Fingerprint method is that to detect the existence of faults or fractures not always related to underground temperature. In the geothermal area, since geothermal fluid is reserved in faults and fractures in the underground, high temperature zone must be the area where geothermal fluid is reserved in faults and fractures.

From the results of fault or fracture detection and underground temperature survey at depth of 100m, it has become clear that high temperature zone with above 60°C coinsides with the area occupied by two faults with NW-SE direction, which means that geothermal fluid is reserved in the faults and fractures with the same direction.

Thus, it can be said that geometry of the geothermal reservoir with wider than 500m and longer than 1,000m has been detected by the supplementary survey carried out in FY 1985. As to the problem whether geothermal development in the San Kampaeng area is feasible or not, fluidal temperature in reservoir has an important role. If geothermal fluid has temperature higher than 180°C, it is possible to construct power plant using geothermal steam, but if the temperature is lower than 180°C, for example, 160 - 180°C, another power generation such as Binary cycle System must be considered.

Consequently, whether geothermal development in the San Kampaeng is feasible or not is due to the fluidal temperature in the reservoir.

Judging from the facts that geochemical thermometer indicated fluidal temperature of 160 - 200°C, and that high temperature was recorded in geothermal manifestation area and in the southern portion of the manifestation area. As conclusion, it can be said that it is worth drilling another exploration well to get the data on fluidal temperature and permeability of the rocks.

5. Selection of drilling site of GTE-8

From the results of the survey carried out in FY 1985, it was concluded that it is necessary to drill another exploration well, GTE-8.

If EGAT will drill GTE-8 in accordance with proposal of the JICA Study Team, drilling site of GTE-8 will be recommended as follows:

There are two selected points as drilling site of GTE-8, one is in and around the geothermal manifestation area, another is in the area including No.9 heat hole. According to the result of Fingerprint method, it seems that predominant fracture system is developed around No. 9 heat hole.

Judging from the topographycal condition, it is recommended that remain of stone pit near No.9 heat hole will be suitable for drilling site.

6. Summary

(1) From the analytical results of logging data, it was deduced that drilling site of GTE-7 is located at recharge area of thermal water.

(2) Also it was deduced that there must be a fault trending from NE to SW between GTE-7 and geothermal manifestation area, separating discharge area from recharge area.

(3) Since useful data to evaluate geothermal reservoir in the San Kampaeng was not obtained from the result of drilling of GTE-7, it was decided that fault or fracture detection and underground temperature survey are carried out in and around geothermal manifestation area to know occurrence of geothermal reservoir in FY 1985.

(4) Fault or fracture detection was carried out by geochemical survey called Fingerprint method. From the result of survey, it was detected that there are two main faults trending from NW to SE located at NE and SE sides of geothermal manifestation area, and another faults trending from NE to SW located north of manifestation area.

(5) Based on the data obtained from drilling of 10 heat holes of 100m deep and measurement of down hole temperature which were carried out by cooperation of EGAT, iso-thermal contour line map at depth of 100m deep was made.

(6) Distribution map of underground temperature is comformable with that of fault or fracture, and it has become clear that high temperature zone with above 70°C occupies the area surrounded by above mentioned two faults with direction of NW - SE, and that geothermal reservoir detected by fault and underground surveys has geometry with wider than 500m and longer than 1,000m.

(7) Whether power generation by using geothermal steam or by Binary Cycle System is feasible or not is due to fluidal temperature in the reservoir. It is considered that, in order to know which is feasible, there is none other useful way than drilling of an exploration well in the survey area.

(8) Judging from estimation of fluidal temperature by chemical thermometer which suggests ranges from 160 to 200°C and records of high underground temperature near surface at geothermal manifestation area and at No.9 heat hole, it concluded that it is worth drilling an exploration well to survey reservoir characteristics.

(9) As drilling site of GTE-8 which is planned to be drilled by EGAT in the near future, it is recommended that remain of stone pit near No. 9 heat hole will be suitable for drilling site of an exploration well.

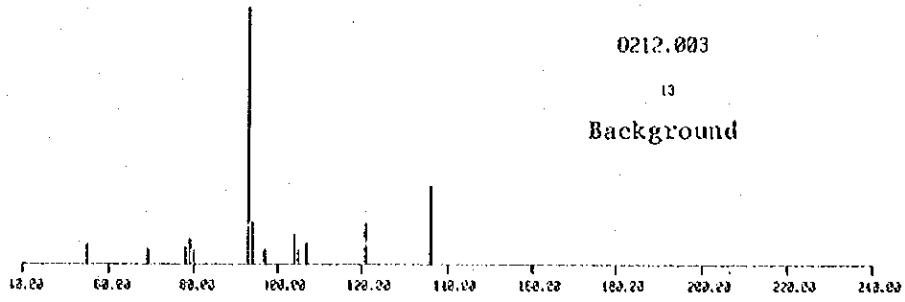

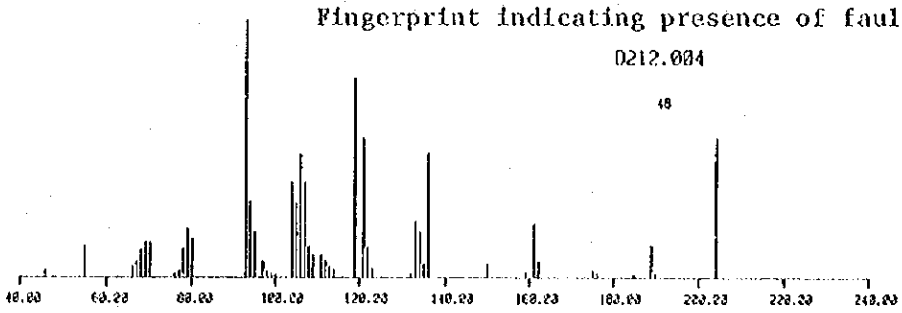

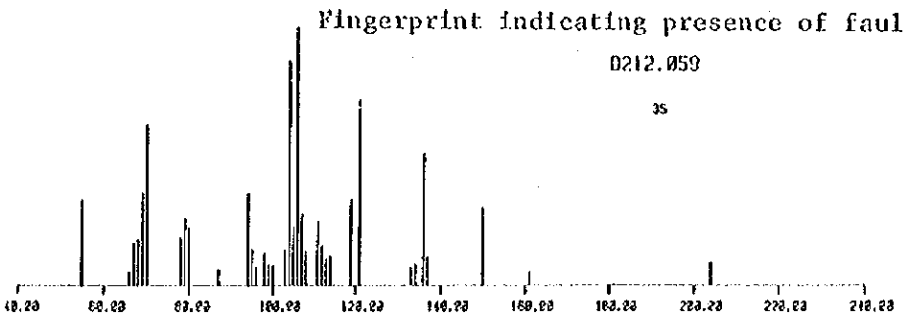

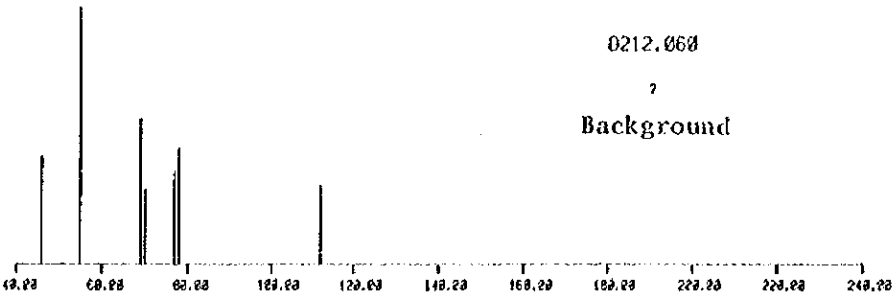

Fig. 19 (1) Fault/fracture and background fingerprint (1)

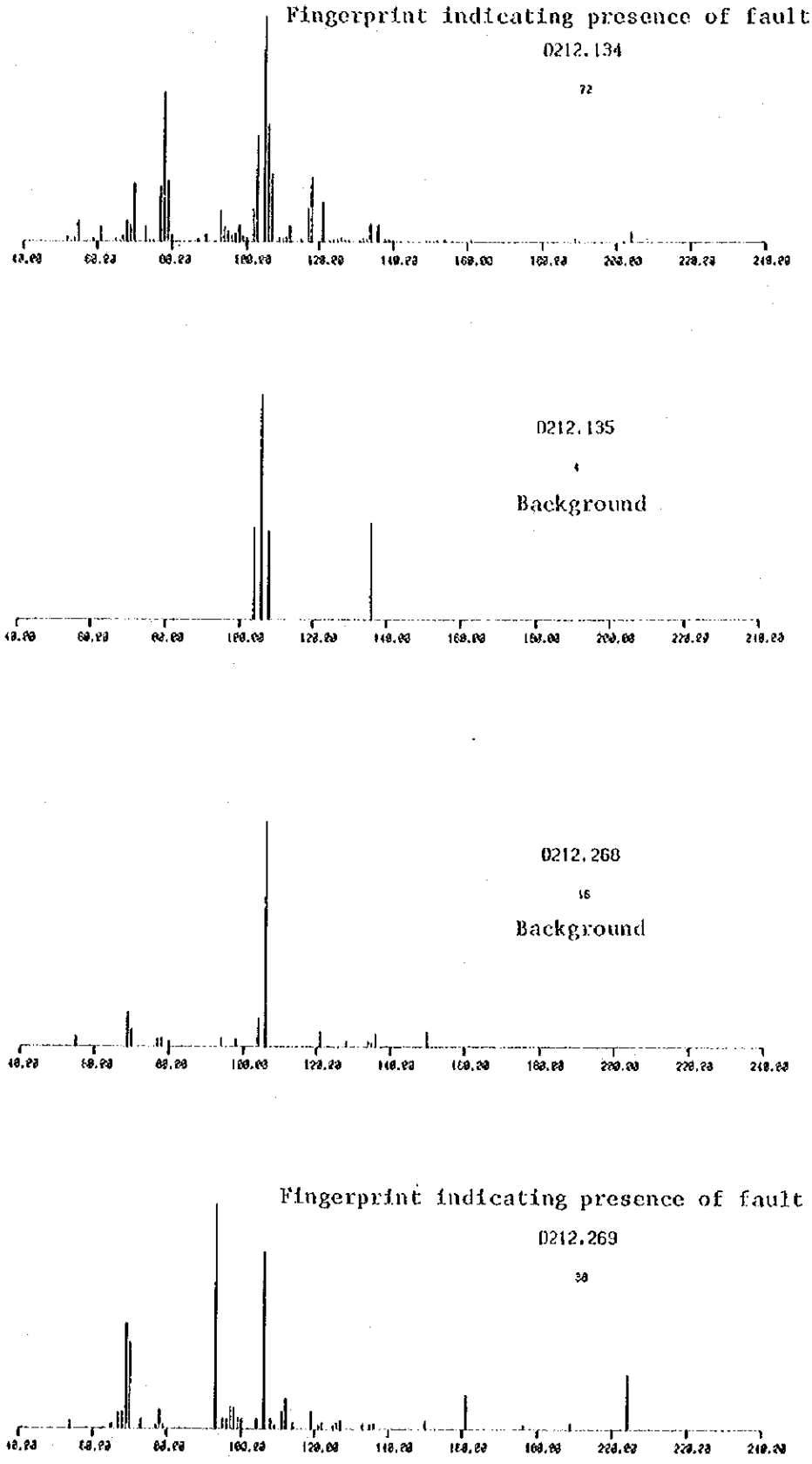

Fig. 19 (2) Fault/fracture and background fingerprint (2)

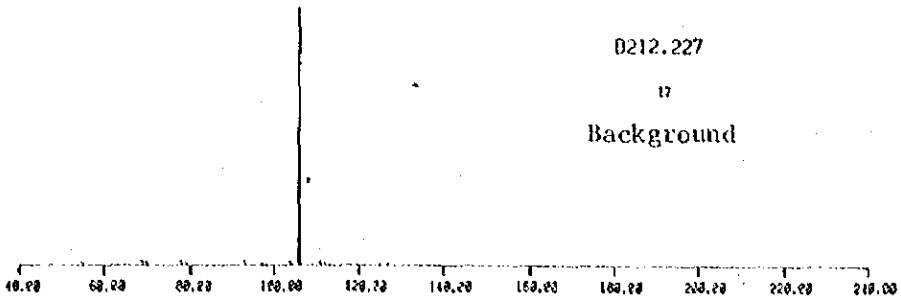

Fingerprint indicating presence of fault

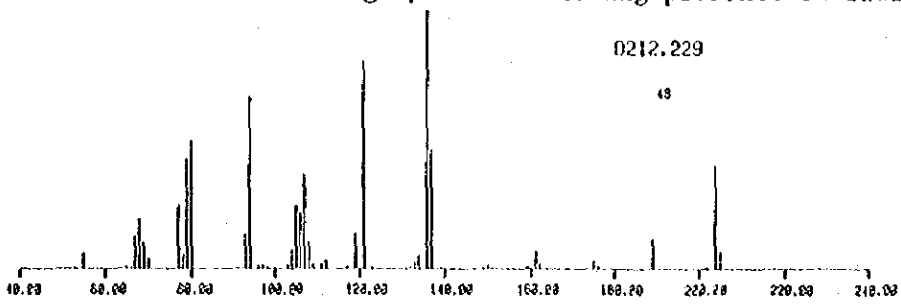

Fingerprint indicating presence of fault

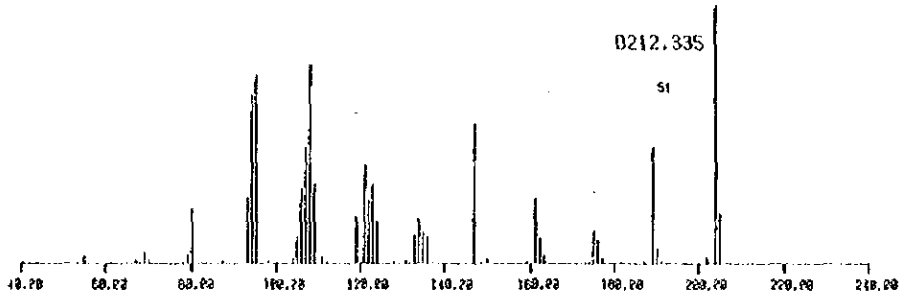

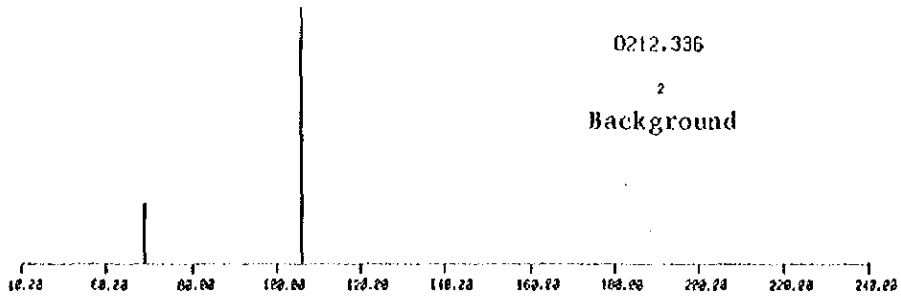

Fig. 19 (3) Fault/fracture and background fingerprint (3)

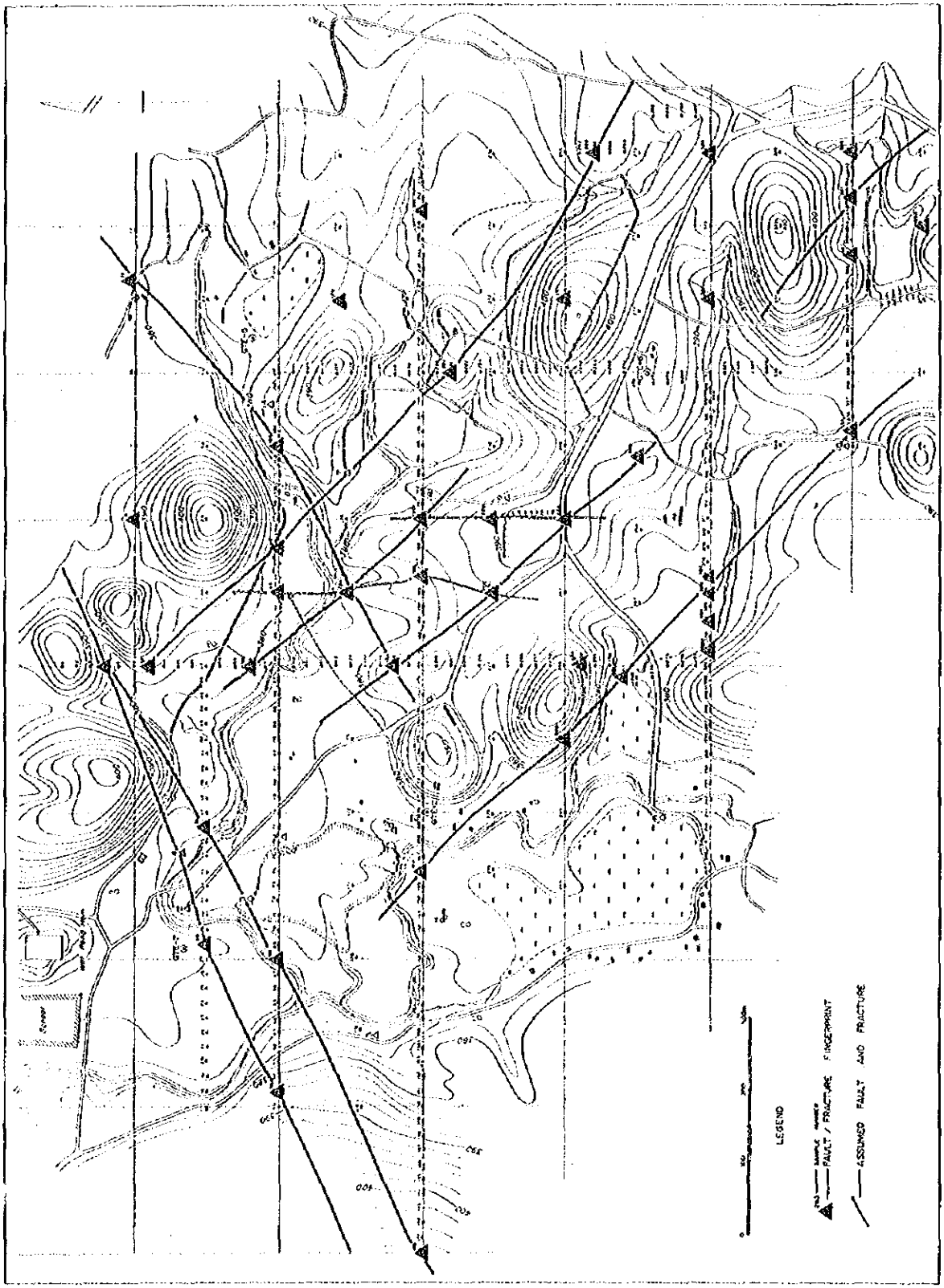

Fig. 20 Distribution map of fault/fracture fingerprint.

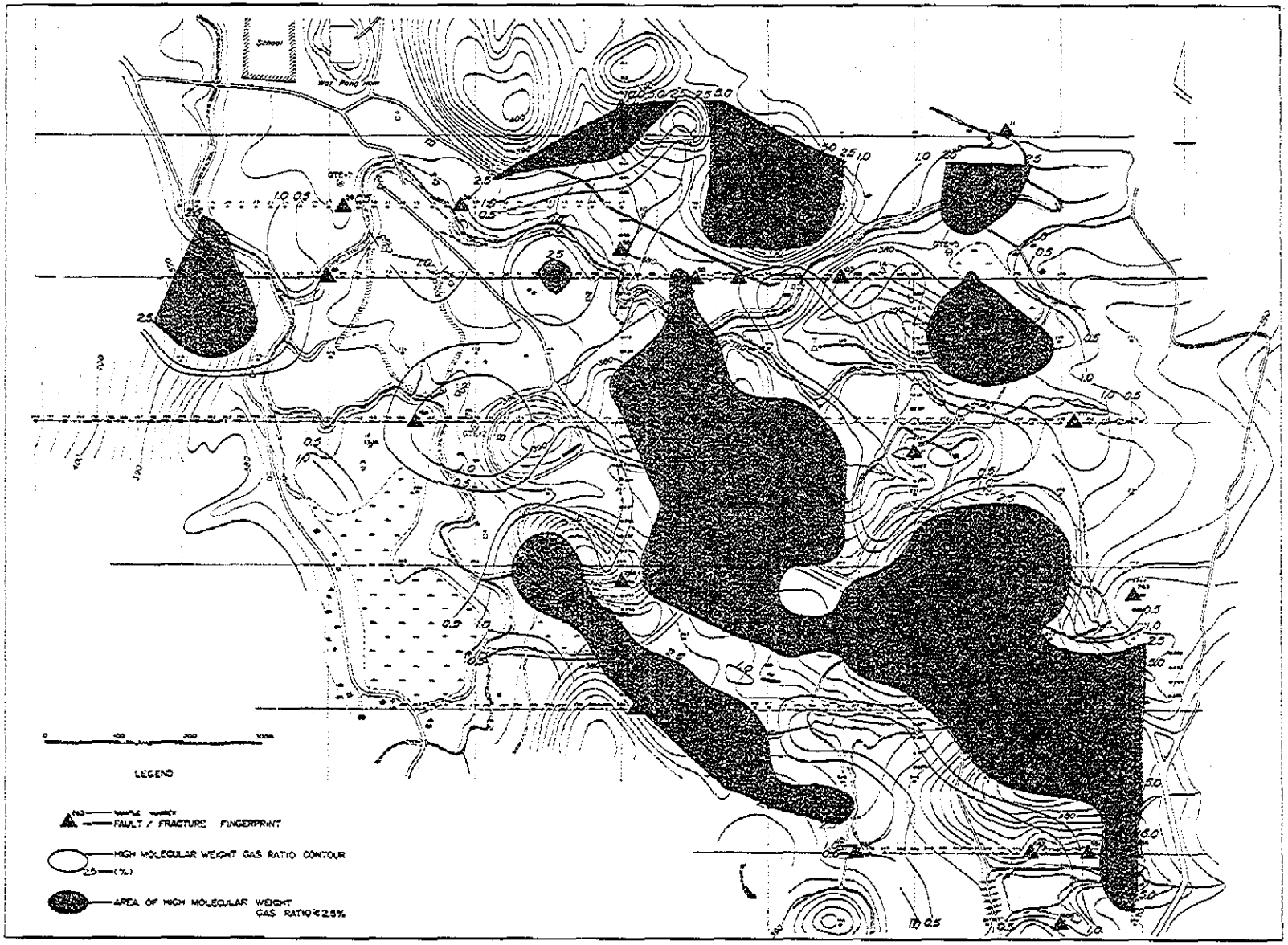

Fig. 21 Contour map of high molecular weight gas ratio.

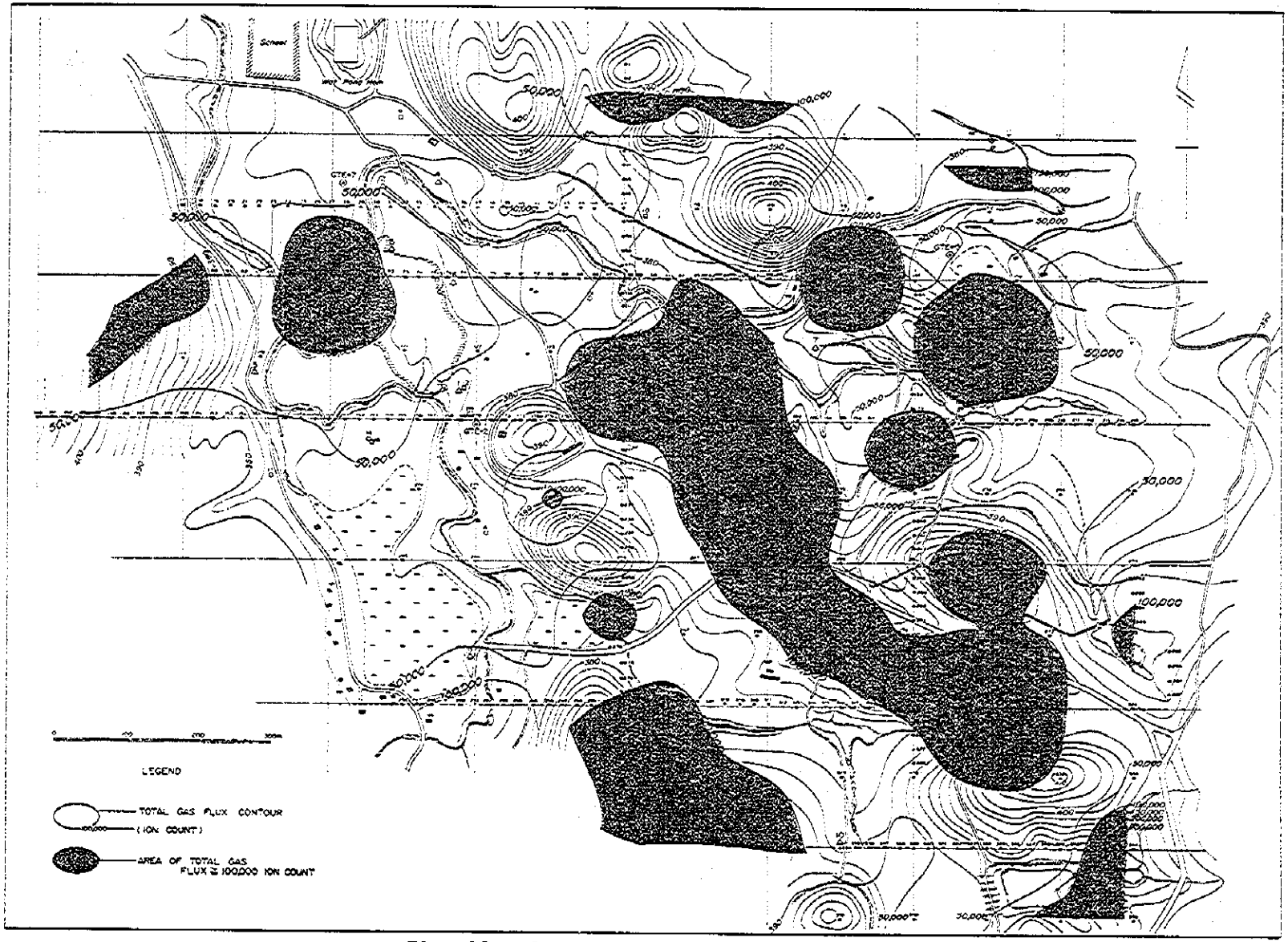

Fig. 22 Contour map of total gas flux

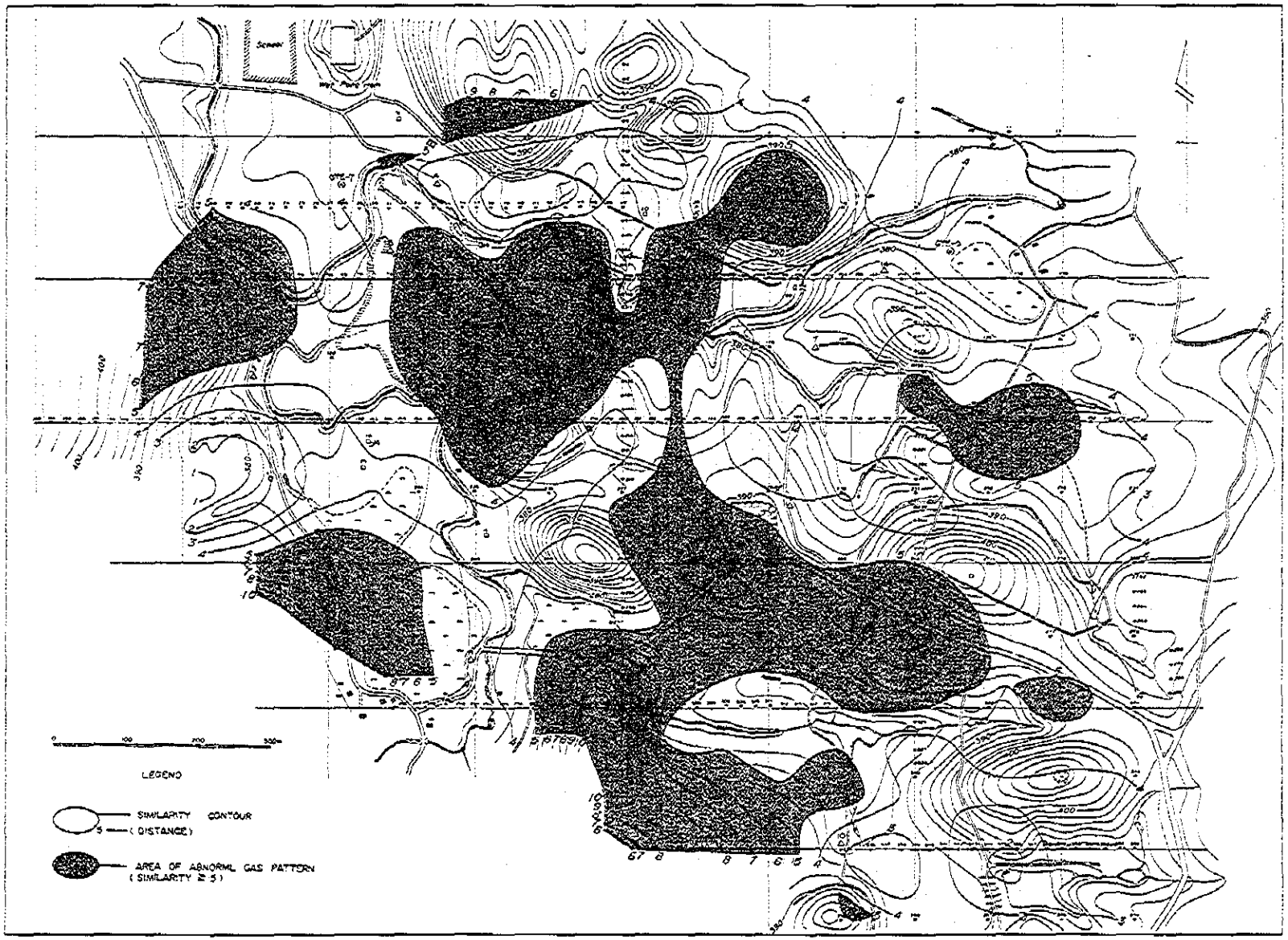

Fig. 23 Similarity map

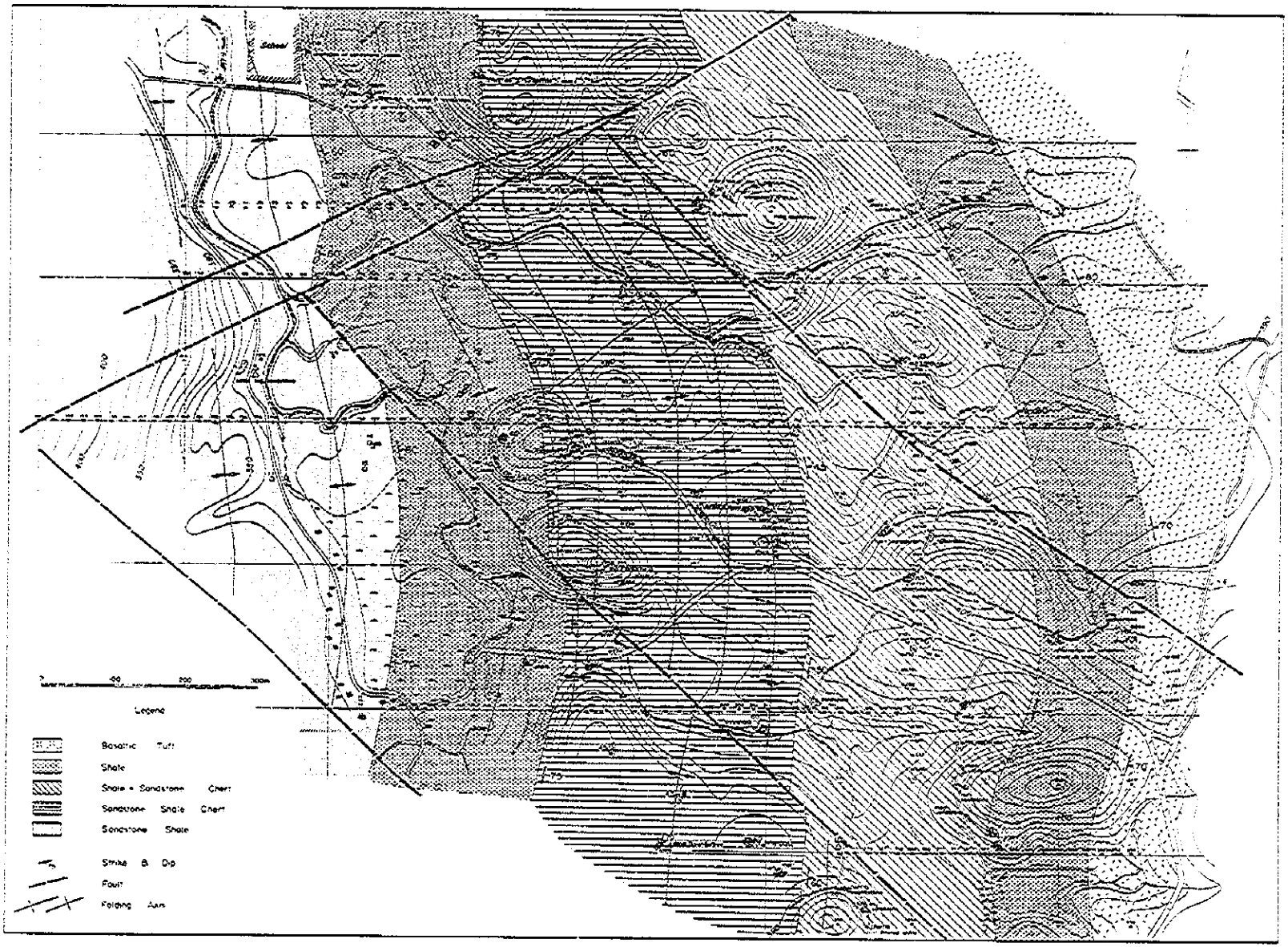

Fig. 24 Geological map

Table 1 Data on bottom of hole temperature in heat holes.

Hole No.	Temperature at bottom of hole (depth)
No. 5	40.3°C (100m)
6	98.2°C (100m)
7	79.6°C (102m)
8	43.6°C (92m)
9	112.3°C (99.5m)
10	62.2°C (102m)
11	78.0°C (92m)
12	40.7°C (100m)
13	37.0°C (100m)
14	48.1°C (94.5m)

Well No.	Down hole temperature at depth of 100m
GTE-2	-
GTE-5	44.2°C
GTE-6	-
GTE-7	60.0°C

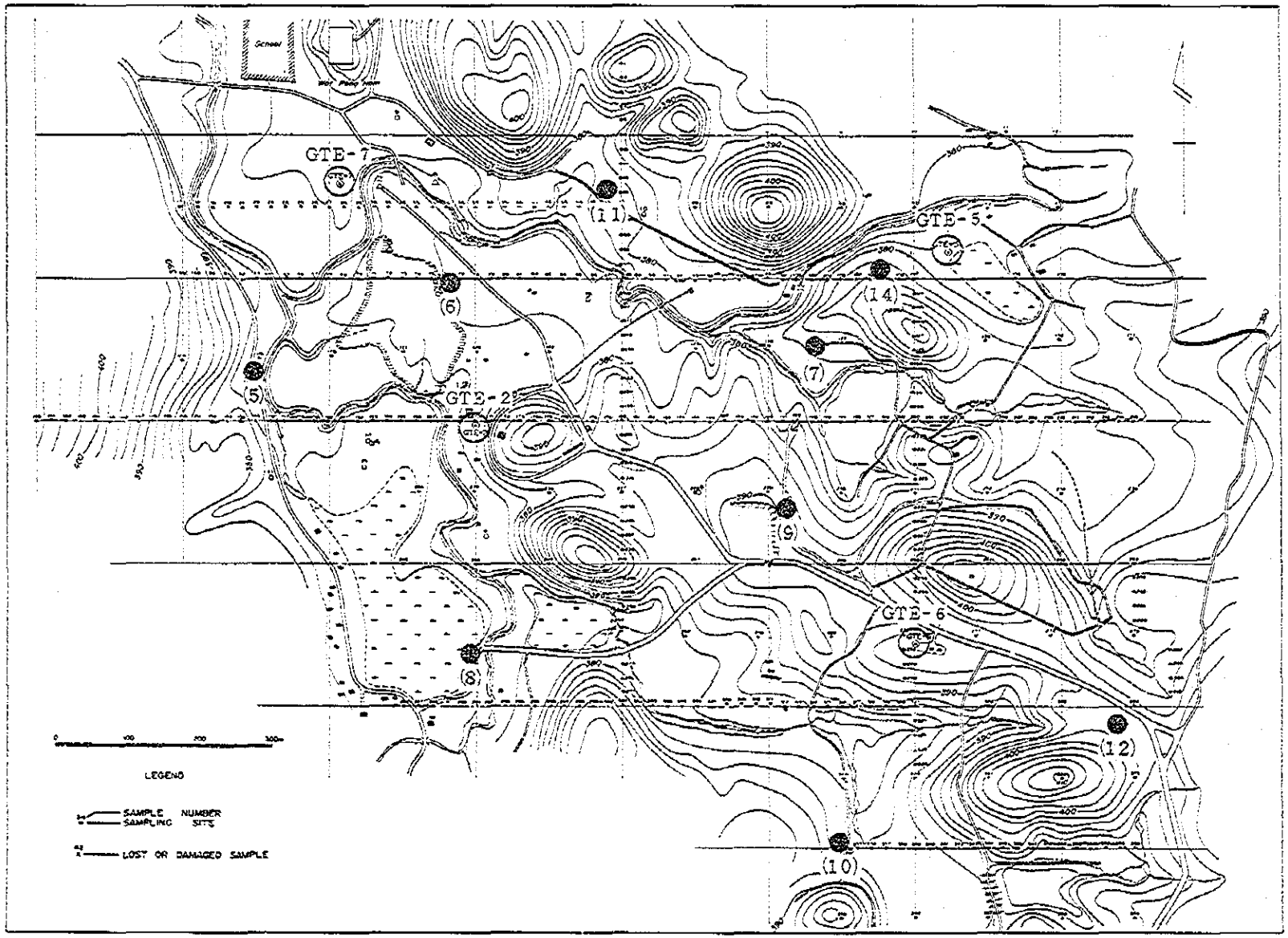

Fig. 25 Locality map of drilling sites of heat holes.

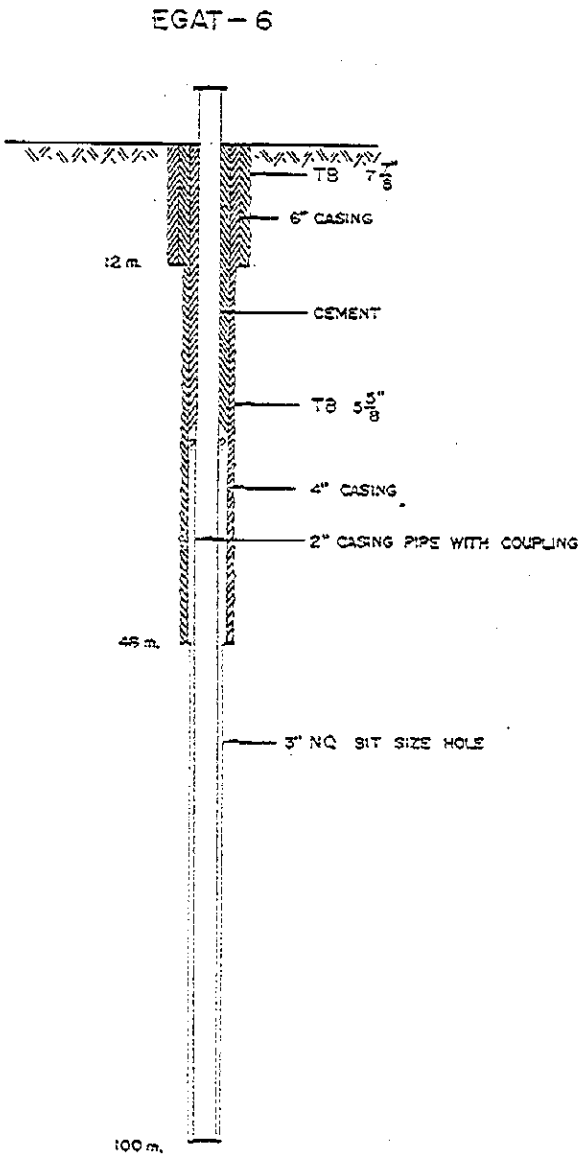

Fig. 26 (1)- Example of completion of heat hole (No.6 Heat Hole).

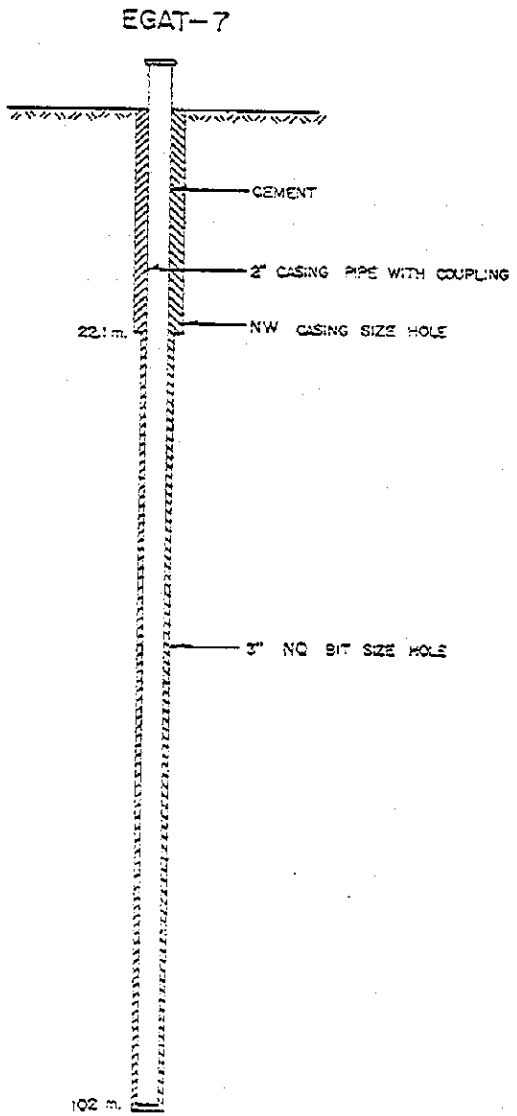

Fig. 26 (2) Example of completion of heat hole (No.7 Heat Hole).

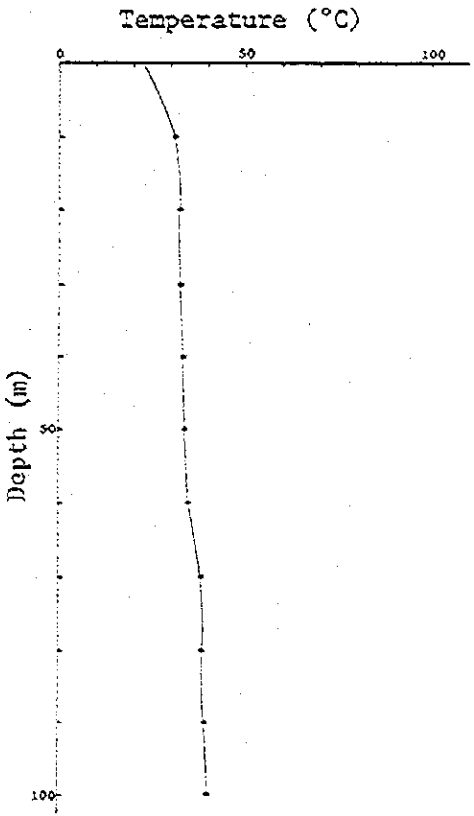

No.5 Heat Hole.

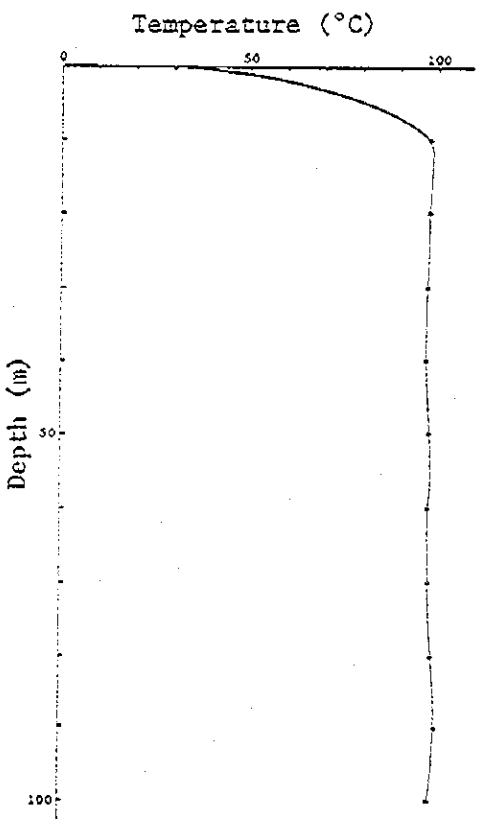

No.6 Heat Hole.

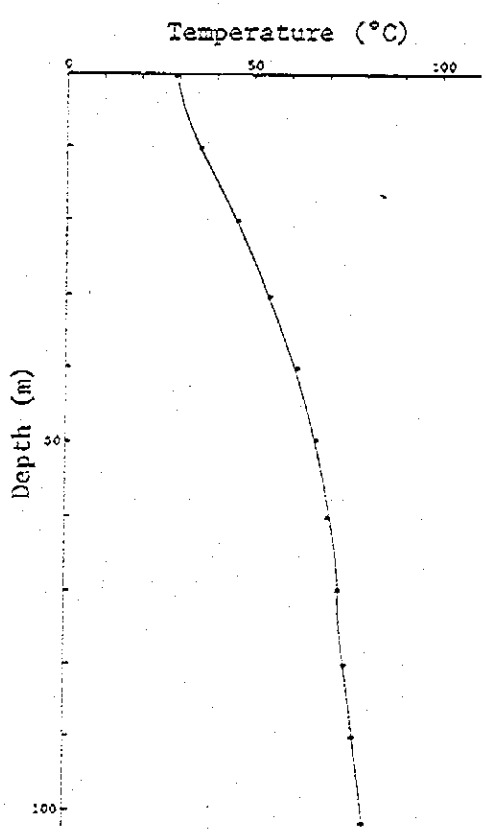

No.7 Heat Hole.

Fig. 27 (1) Down hole temperature distribution

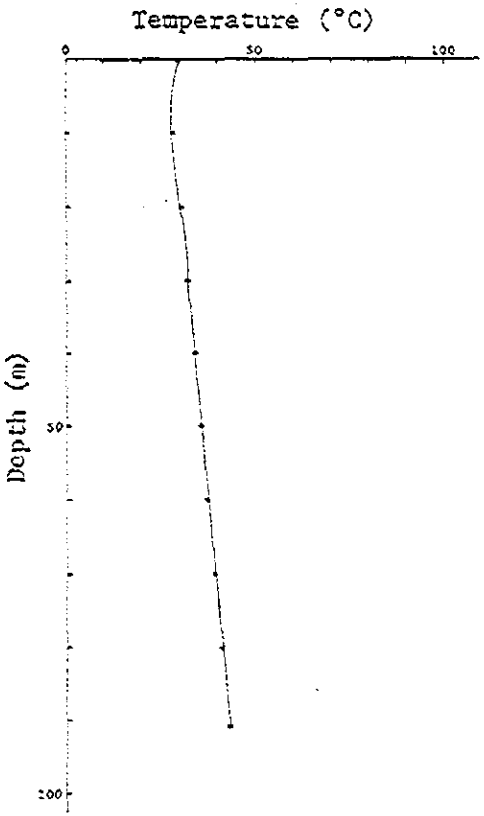

No.8 Heat Hole.

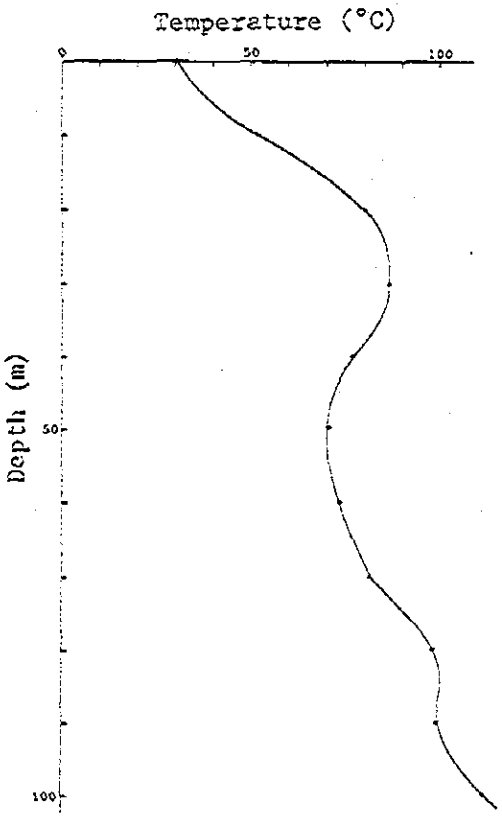

No.9 Heat Hole.

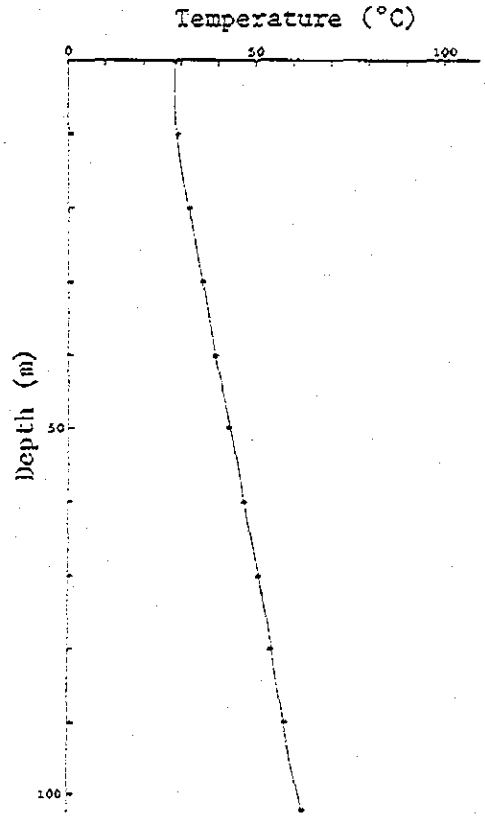

No.10 Heat Hole.

Fig. 27 (2) Down hole temperature distribution

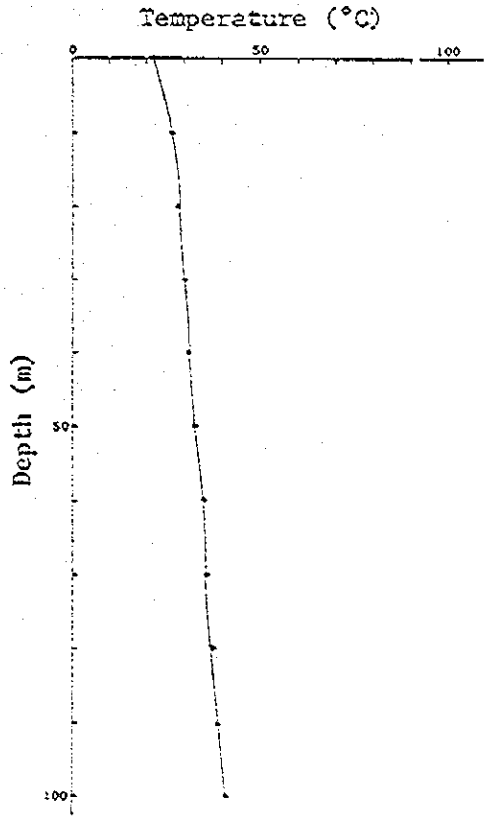

No.12 Heat Hole.

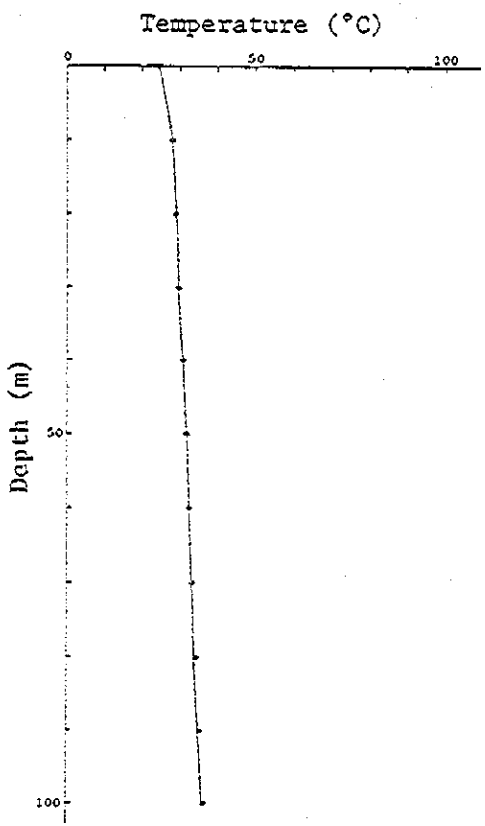

No.13 Heat Hole.

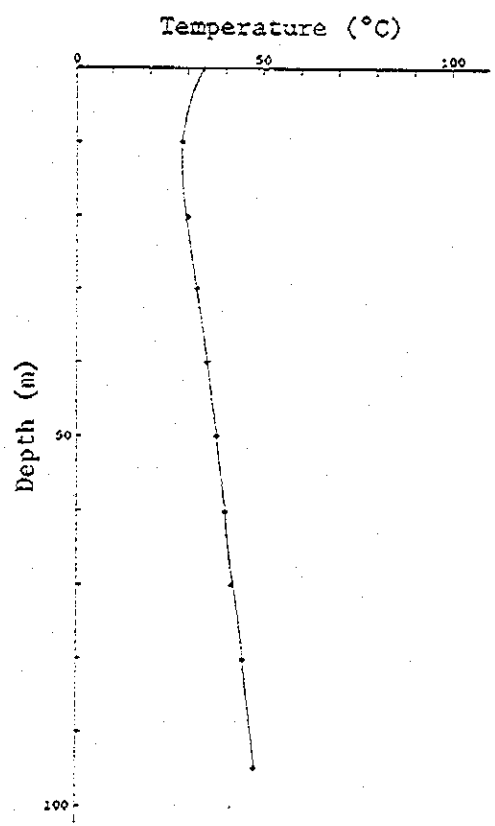

No.14 Heat Hole.

Fig. 27 (3) Down hole temperature distribution

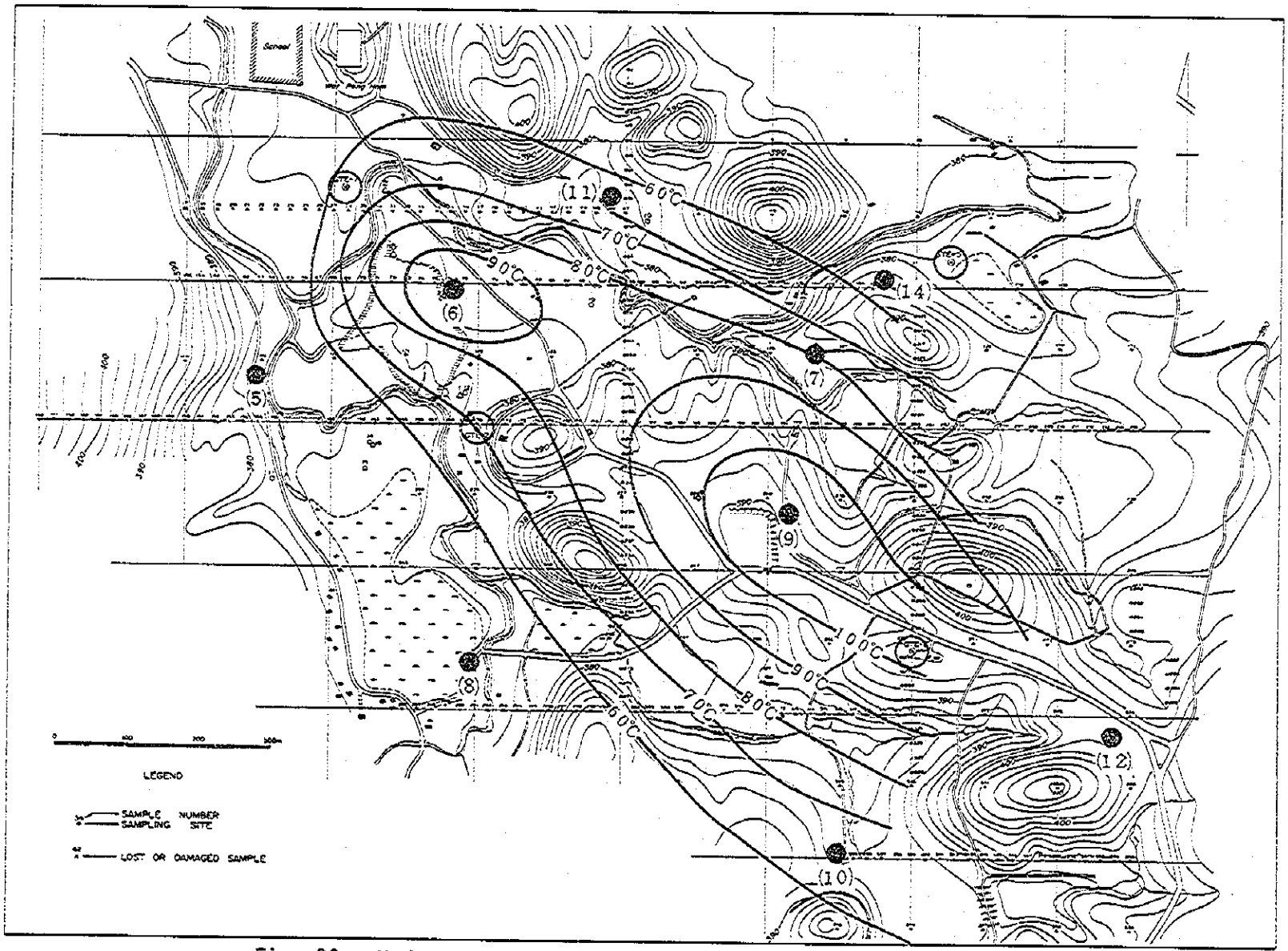

Fig. 28 Underground temperature distribution map at depth of 100m.

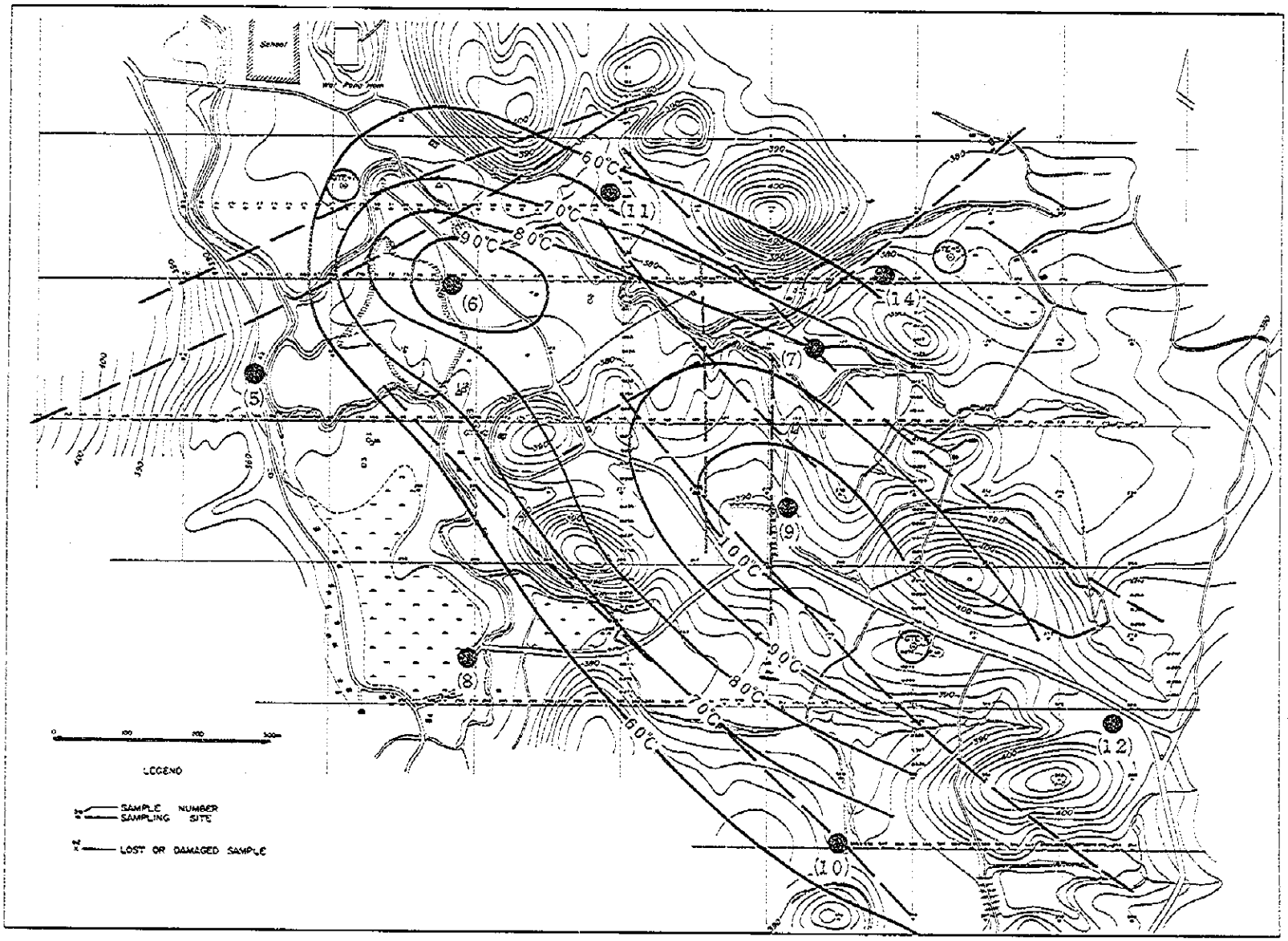

Fig. 29 Relation between fault distribution and underground temperature distribution